Cell Reports

Article

Regulation of STING activity in DNA sensing by ISG15 modification

Graphical abstract

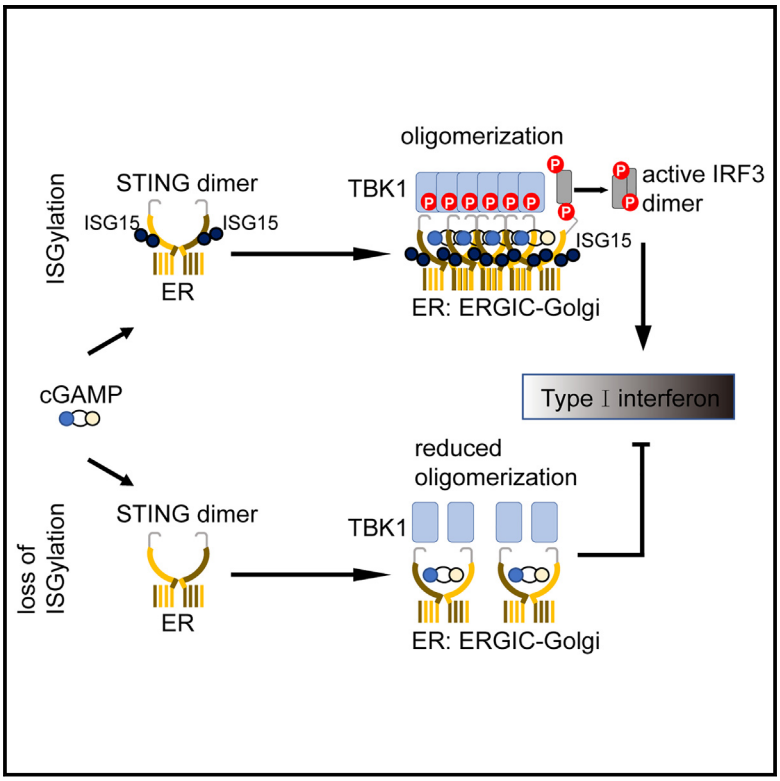

Highlights

- STING is modified by ISG15
- ISGylation of STING at K289 facilitates its oligomerization
- ISG15 deficiency impairs DNA sensing
- SAVI-STING requires ISGylation for constitutive activity

Authors

Chaohui Lin, Edmund Osei Kuffour, Nina V. Fuchs, ..., Holger Gohlke, Renate König, Carsten Münk

Correspondence

carsten.muenk@med.uni-duesseldorf.de

In brief

Lin et al. demonstrate that STING is ISGylated in response to external stimuli. K289-linked ISGylation of STING is essential for interferon induction and STING-dependent autoimmune disease.

Lin et al., 2023, Cell Reports *42*, 113277
November 28, 2023
https://doi.org/10.1016/j.celrep.2023.113277

CellPress

Cell Reports

CellPress
OPEN ACCESS

Article

Regulation of STING activity in DNA sensing by ISG15 modification

Chaohui Lin,[1] Edmund Osei Kuffour,[1,12,13] Nina V. Fuchs,[2] Christoph G.W. Gertzen,[3,4] Jesko Kaiser,[3] Maximilian Hirschenberger,[5] Xiao Tang,[1] Haifeng C. Xu,[6] Oliver Michel,[3] Ronny Tao,[7] Alexandra Haase,[8,9] Ulrich Martin,[8,9,10] Thomas Kurz,[3] Ingo Drexler,[7] Boris Görg,[1] Philipp A. Lang,[6] Tom Luedde,[1] Konstantin M.J. Sparrer,[5] Holger Gohlke,[3,11] Renate König,[2] and Carsten Münk[1,14,*]

[1]Clinic of Gastroenterology, Hepatology and Infectious Diseases, Medical Faculty, Heinrich Heine University Düsseldorf, Düsseldorf, Germany
[2]Host-Pathogen Interactions, Paul-Ehrlich-Institut, Langen, Germany
[3]Institute for Pharmaceutical and Medicinal Chemistry, Heinrich Heine University Düsseldorf, Düsseldorf, Germany
[4]Center for Structural Studies (CSS), Heinrich Heine University Düsseldorf, Düsseldorf, Germany
[5]Institute of Molecular Virology, Ulm University Medical Center, 89081 Ulm, Germany
[6]Department of Molecular Medicine II, Medical Faculty, Heinrich Heine University Düsseldorf, Düsseldorf, Germany
[7]Institute for Virology, Medical Faculty, Heinrich Heine University Düsseldorf, Düsseldorf, Germany
[8]Leibniz Research Laboratories for Biotechnology and Artificial Organs (LEBAO), Department of Cardiothoracic, Transplantation and Vascular Surgery (HTTG), Hannover Medical School, 30625 Hannover, Germany
[9]REBIRTH-Research Center for Translational and Regenerative Medicine, Hannover Medical School, 30625 Hannover, Germany
[10]Biomedical Research in Endstage and Obstructive Lung Disease (BREATH), Member of the German Center for Lung Research (DZL), Hannover Medical School, 30625 Hannover, Germany
[11]Institute of Bio- and Geosciences (IBG-4: Bioinformatics), Forschungszentrum Jülich GmbH, 52425 Jülich, Germany
[12]Present address: Laboratory of Retrovirology, The Rockefeller University, New York, NY 10065, USA
[13]Present address: Howard Hughes Medical Institute, The Rockefeller University, New York, NY 10065, USA
[14]Lead contact
*Correspondence: carsten.muenk@med.uni-duesseldorf.de
https://doi.org/10.1016/j.celrep.2023.113277

SUMMARY

Sensing of human immunodeficiency virus type 1 (HIV-1) DNA is mediated by the cyclic GMP-AMP synthase-stimulator of interferon genes (cGAS-STING) signaling axis. Signal transduction and regulation of this cascade is achieved by post-translational modifications. Here we show that cGAS-STING-dependent HIV-1 sensing requires interferon-stimulated gene 15 (ISG15). ISG15 deficiency inhibits STING-dependent sensing of HIV-1 and STING agonist-induced antiviral response. Upon external stimuli, STING undergoes ISGylation at residues K224, K236, K289, K347, K338, and K370. Inhibition of STING ISGylation at K289 suppresses STING-mediated type I interferon induction by inhibiting its oligomerization. Of note, removal of STING ISGylation alleviates gain-of-function phenotype in STING-associated vasculopathy with onset in infancy (SAVI). Molecular modeling suggests that ISGylation of K289 is an important regulator of oligomerization. Taken together, our data demonstrate that ISGylation at K289 is crucial for STING activation and represents an important regulatory step in DNA sensing of viruses and autoimmune responses.

INTRODUCTION

The innate immune system is the first line of defense against invading pathogens.[1] It relies on conserved germline-encoded pattern-recognition receptors (PRRs) that detect defined pathogen-associated molecular patterns (PAMPs) generated during microbial infection.[2] A major component of PAMP is viral nucleic acid intermediates generated during virus replication.[3] Several classes of PRRs, including Toll-like receptors (TLRs), RIG-I-like receptors, and cytosolic DNA sensor molecules have been described.[3,4] For example, cytosolic DNA is sensed by a variety of cytosolic DNA sensors, the most prominent among them is the cyclic GMP-AMP synthase (cGAS).[3,5] The recognition of viral nucleic acids by PRRs recruits adaptor molecules or kinases to activate transcription factors that regulate the production of proinflammatory cytokines and type I interferons (IFNs).[3,4] cGAS binds to cytosolic DNA and produces cyclic GMP-AMP (cGAMP), which binds to the adaptor protein stimulator of interferon genes (STING) residing in its inactive form at the endoplasmic reticulum (ER).[5–10] Subsequently, STING undergoes a conformational change and enhanced oligomerization to initiate signaling.[7,10,11] Activated STING is transported to the Golgi to promote binding to TANK-binding kinase 1 (TBK1), which phosphorylates interferon regulatory factor 3 (IRF3) and nuclear factor of kappa light polypeptide gene enhancer in B cells inhibitor alpha (IκBα) to release nuclear factor kappa B (NF-κB).[12–15] The transcription factors then induce type I IFN and proinflammatory cytokines to counteract infection.[14] Consistently,

STING deficiency abrogates cytosolic DNA-sensing-mediated *IFNB1* mRNA expression.[16] STING-deficient mice present decreased IFN responses and impaired T cell immunity upon viral infection.[17,18] Vice versa, gain-of-function heterozygous mutations in the human *STING* gene have been linked to autoinflammatory diseases such as STING-associated vasculopathy with onset in infancy (SAVI) and familial chilblain lupus.[19] For example, the mutation V155M in human STING activates STING independently of its ligand cGAMP, leading to chronic IFN release and induction of interferon-stimulating genes (ISGs).[20,21]

Post-translational modification (PTM) including phosphorylation, ubiquitination, palmitoylation, and SUMOylation have been reported to play an essential role in regulating STING function.[22] For example, the E3 ligases tripartite motif containing 56 (TRIM56), TRIM32, TRIM10, and autocrine motility factor receptor (AMFR) have been proposed to catalyze K63-, K27-, or K29-linked polyubiquitination to boost STING signaling.[23–26] SUMOylation of STING promotes its stability to enhance the immune response to DNA virus early infection.[27] Palmitoylated STING at the Golgi is important for its activation and recruitment of TBK1 and IRF3.[28] Whether other types of PTMs are associated with the regulation of STING is currently unclear.

ISG15 is a ubiquitin-like molecule that is highly induced by type I IFN during the infection of human cells by viral and bacterial pathogens.[29,30] During ISG15 modification (also termed ISGylation), the carboxy-terminal LRLRGG motif of ISG15 is covalently conjugated to the lysine residues of intracellular proteins.[30] Similar to ubiquitin ligation, the process of ISGylation occurs through a three-step enzymatic cascade, involving ubiquitin-activating enzyme E1-like protein (UBE1L), conjugating E2 enzyme ubiquitin-conjugating human enzyme 8 (UBCH8), and one of three E3 ligases, HERC domain and RCC1-like domain-containing protein 5 (HERC5), tripartite motif containing 25 (TRIM25, also known as EFP), or human homolog of *Drosophila ariadne* (ARIH1).[31–38] Mice lacking UBE1L or ISG15 are more susceptible to viral infection, indicating that ISGylation is involved in modulating antiviral immunity.[39,40] Several studies have found that ISG15 exhibits antiviral activity by conjugating to both viral and host proteins.[41] The capsid protein L1 of human papillomavirus can be ISGylated and then incorporated into viral particles, which reduces the rate of viral budding.[42] ISGylation of host tumor susceptibility gene 101 protein (TSG101) disrupts the HIV-1 Gag-TSG101 interaction and consequently decreases HIV-1 release.[43] The ISGylation of IRF3 enhances cellular antiviral responses, whereas ISGylation of retinoic acid-inducible gene I (RIG-I) reduced levels of both basal and virus-induced IFN promoter activity.[44,45] ISG15 conjugation is vital for antiviral IFN responses mediated by the viral RNA sensor melanoma differentiation-associated protein 5 (MDA5), which promotes its oligomerization and thereby triggers antiviral immunity.[46] ISGylation of cGAS inhibits its optimal activation and DNA-induced oligomerization.[47] Thus, ISGylation has varying impacts on innate immunity depending on the targeted protein and context. Conjugated ISG15 can be reversed by the ubiquitin-specific peptidase 18 (USP18) that cleaves ISG15-peptide linkages.[48] In addition, the papain-like protease (PLpro, the protease domain of Nsp3) of SARS-CoV-2, cleaves ISG15 from IRF3 and MDA5, thereby attenuating the type I IFN response in the setting of infection.[46,49]

Here, we identified that the DNA sensing adaptor STING is modified by ISG15 in response to viral infection or cytosolic DNA simulation and that this modification promotes STING-triggered innate immune response. Knockout of ISG15 impairs the sensing of HIV-1 and attenuates cellular antiviral responses. Removal of ISG15 from STING reverses chronic inflammation in STING-dependent autoimmune disorder.

RESULTS

ISG15 deficiency enhances HIV-1 infection by impairing sensing of HIV-1

To address the functional impact of ISG15 in HIV-1 infection and sensing, we generated ISG15-deficient THP-1 cells using the CRISPR-Cas9 system (Figure 1A).[50] Consistent with our previous observations,[50] our data showed that the infection of HIV-1 was enhanced in both undifferentiated and phorbol-12-myristat-13-acetat (PMA)-differentiated ISG15-deficient THP-1 cells compared with vector control THP-1 cells (pLentiCRISPRv2 empty vector [pLV2]) (Figure 1B). To investigate whether ISG15 modulates the antiviral immune response against HIV-1, we evaluated the presence of IFN in the supernatant of ISG15-deficient and vector control THP-1 cells upon infection. Compared with the vector control THP-1 cells, ISG15 deficiency abrogated HIV-1-triggered type I IFN induction (Figure 1C). Furthermore, we found that knockout of ISG15 significantly impaired HIV-1-induced robust expression of IRF3-dependent target gene *ISG54,*[51] indicating that ISG15 is essential for HIV-1-triggered innate responses (Figure 1D). These data suggest that ISG15 deficiency impairs the sensing of HIV-1 and thus enhances HIV-1 infection.

ISG15 deficiency suppresses STING-dependent DNA sensing

Sensing of HIV-1 cDNA by cGAS-STING signaling has emerged as a major sensing pathway in mounting the antiviral immune response toward the infection.[52,53] Consistent with the observations using HIV-1, ISG15 deficiency inhibited the induction of type I IFN triggered by other DNA viruses such as modified vaccinia virus Ankara (MVA) or transfected herring sperm (HS)-DNA (Figure 2A). In addition, knockout of ISG15 substantially inhibited the expression of *IFNB1*, *ISG54*, and *TNF-α* after transfection of HS-DNA (Figure 2B). Previous reports identified STING agonists that bypass cGAS to activate innate immune responses.[54,55] We next tested whether ISG15 is involved in STING agonists-triggered activation of the innate immune response. Using the potent STING agonists SR-717,[54] the induction of type I IFN and *IFNB1*, *ISG54*, and *TNF-α* mRNAs was almost completely abolished in ISG15 knockout THP-1 cells compared with vector control cells (Figures 2C and 2D). Subsequently, we examined the antiviral function of the STING agonist SR-717 treatment in ISG15 knockout THP-1 cells. The absence of ISG15 abrogated the SR-717-induced inhibition of HIV-1 infection due to the impaired induction of IFNs (Figures 2E and 2F). Together, these data suggest that ISG15 is required for STING-dependent induction of innate immune responses.

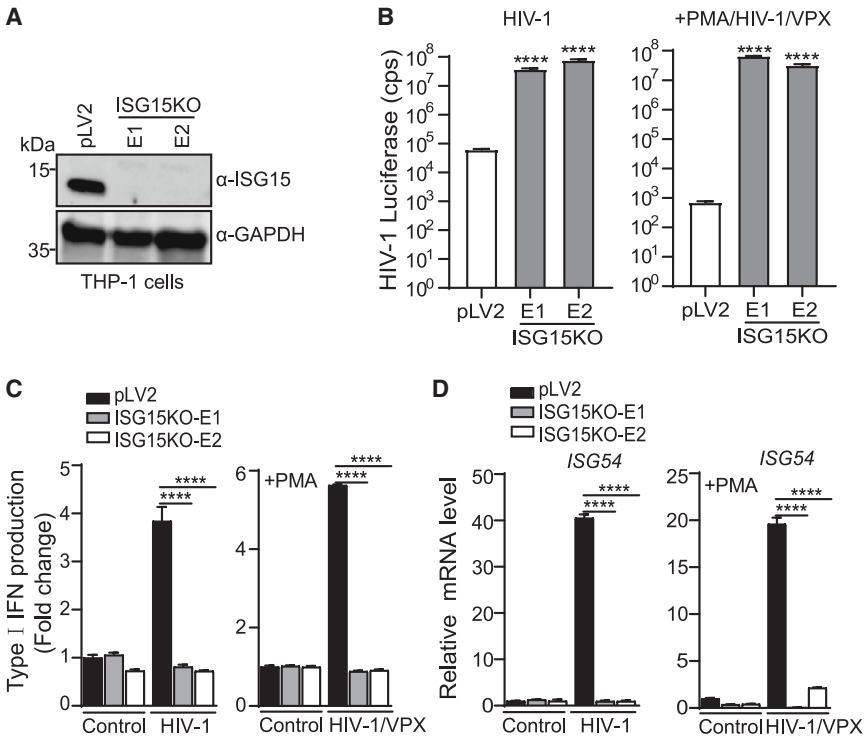

Figure 1. ISG15 deficiency impairs sensing of HIV-1

(A) Immunoblot analysis of ISG15 and GAPDH in THP-1.pLV2 (pLentiCRISPRv2 empty vector [pLV2]) and THP-1.ISG15KO-E1/E2 cells (pLentiCRISPRv2 with sgRNAs targeting exons 1/2 of the *ISG15* gene).

(B and C) Undifferentiated or phorbol-12-myristate-13-acetate (PMA)-differentiated THP-1.ISG15KO-E1/E2 and THP-1.pLV2 cells were transduced with HIV-1 luciferase reporter virus with or without the copackaged lentiviral accessory protein VPX for 72 h, followed by luciferase activity analysis (B) and type I interferon production analysis (C).

(D) RT-qPCR analysis of *ISG54* mRNA in undifferentiated or PMA-differentiated THP-1.ISG15KO-E1/E2 and THP-1.pLV2 cells that were transduced with HIV-1 luciferase reporter virus with or without the copackaged VPX for 24 h. *GAPDH* served as housekeeping gene. Significance was determined using one-way analysis of variance (-ANOVA) (*$p < 0.05$, **$p < 0.01$, ***$p < 0.001$, and ****$p < 0.0001$). Data are representative of three independent experiments (graphs show mean ± SD in Figures 1B–1D).

STING is modified by ISG15

Current studies have identified a role of ISG15 in the enhancement of antiviral response through ISGylation of cGAS, MDA5, and IRF3.[44,46,47] However, whether STING is ISGylated is currently unknown. To test STING ISGylation, we co-expressed STING-HA (STING with an HA tag), ISG15, UBE1L (E1), and UBCH8 (E2), in the presence of either USP18 or its catalytic mutants (C64A and C64S). After immunoprecipitation of STING-HA, robust ISGylation of STING was detectable by anti-ISG15 and anti-STING antibodies (Figure 3A). Importantly, the ISGylation of STING was abolished by USP18 co-expression, but not by co-expression of the inactive variants USP18-C64A or USP18-C64S (Figure 3A). In the IPs, in comparison with the wild-type USP18 or USP18-C64A, the levels of unconjugated ISG15 in co-expression with STING and ISG15 are higher in the presence of USP18-C64S, which correlated with increased binding of USP18-C64S to both STING and free ISG15 (Figure 3A).[56] In addition to USP18, SARS-CoV-2-Nsp3 PLpro protease removed the ISGylation of STING (Figure 3B), which is consistent with its suppressive de-ISGylation activity on MDA5 and IRF3.[46,49] STING knockout THP-1 cells were reconstituted with wild-type STING-HA or empty vector (pEV) control to further validate this finding. These cells were stimulated with IFN-β and STING-HA was purified. Of note, we observed high-molecular-weight species reactive to anti-ISG15 and anti-STING antibodies in STING-HA-expressing THP-1 cells, which were absent in the empty vector control THP-1 cells (pEV) (Figure 3C). This indicated that stably expressed STING is ISGylated. Additionally, our cell models demonstrated expression of the endogenous E3 ligases HERC5, ARIH1, and TRIM25 (Figures 3A and 3C). To determine whether STING ISGylation is induced in response to other external stimuli, we transfected STING-expressing THP-1 cells with HS-DNA, treated with IFN-β, or infected with HIV-1. Interestingly, STING is ISGylated in response to all the external stimuli tested, but with various amounts (Figure 3D). Furthermore, we tested whether also endogenous STING is modified by ISG15. Anti-ISG15 and anti-STING immunoblots of immunoprecipitated endogenous ISG15 or STING from wild-type THP-1 cells that were stimulated with IFN-β or transfected with the HS-DNA showed ISGylation of STING (Figures 3E and 3F). Taken together, our results suggest that STING is ISGylated in response to cytosolic DNA stimulation and viral infection.

STING residues K224, K236, K289, K338, K347, and K370 are modified by ISG15

ISG15 uses its C-terminal glycine to covalently bind a lysine (K) of the target protein.[30] To identify the ISG15 conjugation sites of STING, we constructed plasmids expressing lysine-free STING (STING-K0 with all K to A mutated). STING ISGylation was completely abolished in STING-K0 (Figure 4A). Next, individual lysines were reintroduced back into the K0 mutant. ISGylation reappeared in STING K0 mutants in which A224, A236, A289, A338, A347, or A370 was restored to K, and these ISG15 modifications were abrogated in the presence of USP18 (Figure 4A). To rule out structural alterations in STING due to the K to A mutations, single or multiple lysine to arginine (R) mutations were generated in STING. The STING ISGylation was almost completely abolished when the six lysines together (K224,

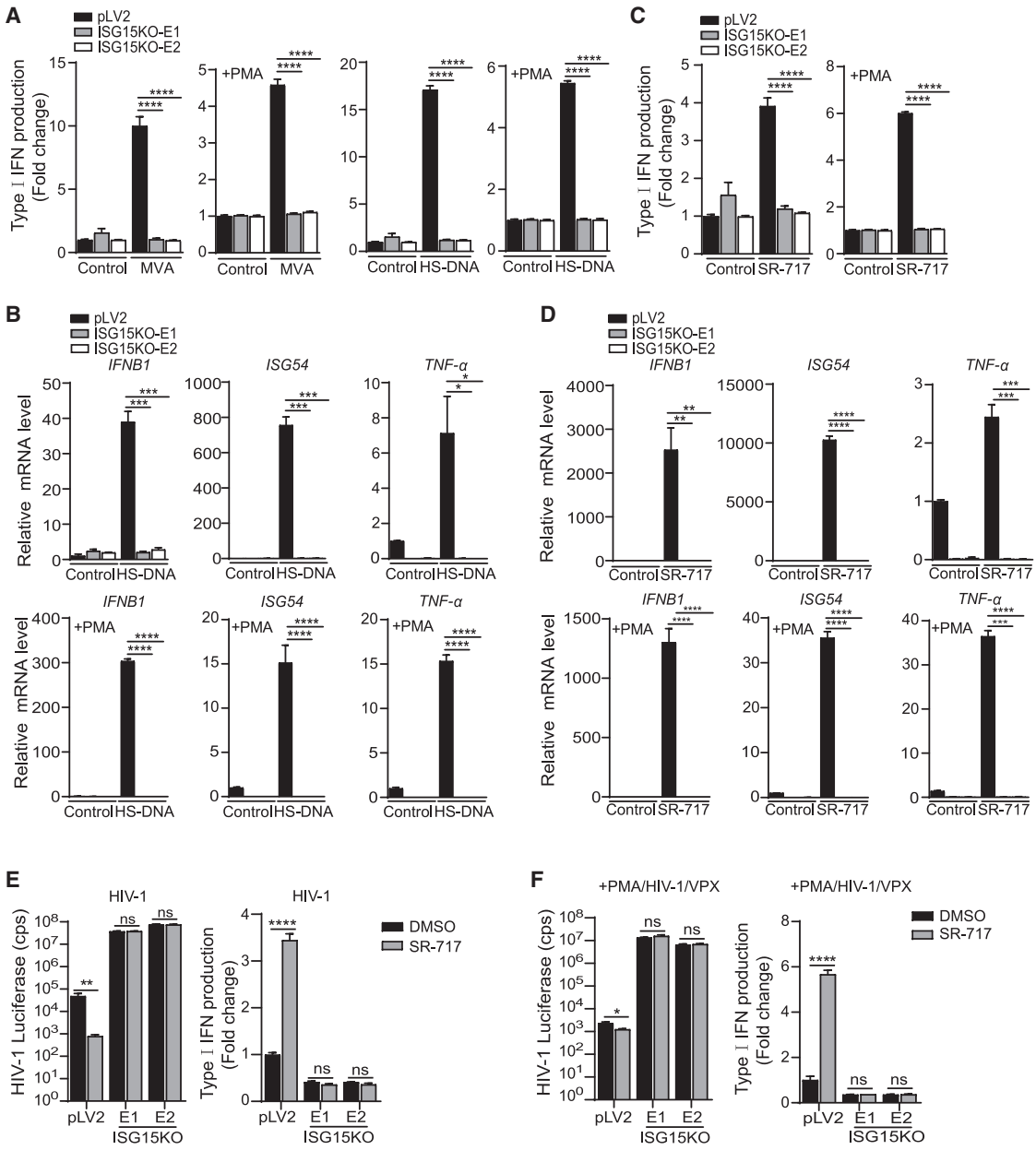

Figure 2. ISG15 deficiency suppresses DNA sensing

(A) Undifferentiated or PMA-differentiated THP-1.ISG15KO-E1/E2 and THP-1.pLV2 cells were infected with MVA or transfected with 4 μg/mL HS-DNA for 48 h followed by type I interferon production analysis.

(B) RT-qPCR analysis of *IFNB1*, *ISG54*, and *TNF-α* mRNA in undifferentiated or PMA-differentiated THP-1.ISG15KO-E1/E2 and THP-1.pLV2 cells that were transfected with 4 μg/mL HS-DNA for 24 h. *GAPDH* served as housekeeping gene.

(C) Undifferentiated or PMA-differentiated THP-1.ISG15KO-E1/E2 and THP-1.pLV2 were stimulated with 3.6 μM SR-717 for 48 h followed by type I interferon production analysis.

(D) RT-qPCR analysis of *IFNB1*, *ISG54*, and *TNF-α* mRNA in undifferentiated or PMA-differentiated THP-1.ISG15KO-E1/E2 and THP-1.pLV2 cells that were stimulated with 3.6 μM SR-717 for 2 h. *GAPDH* served as housekeeping gene.

(E and F) Undifferentiated (E) or PMA-differentiated (F) THP-1.ISG15KO-E1/E2 and THP-1.pLV2 cells were treated with 3.6 μM SR-717 or DMSO for 12 h and then were transduced with HIV-1 luciferase reporter virus with or without the copackaged VPX for 72 h followed by luciferase activity analysis and type I interferon production analysis. Significance was determined using one-way ANOVA (Figures 2A–2D) or two-tailed Student's t test (Figures 2E and 2F) (ns, not significant; *p < 0.05, **p < 0.01, ***p < 0.001, and ****p < 0.0001). Data are representative of three independent experiments (graphs show mean ± SD).

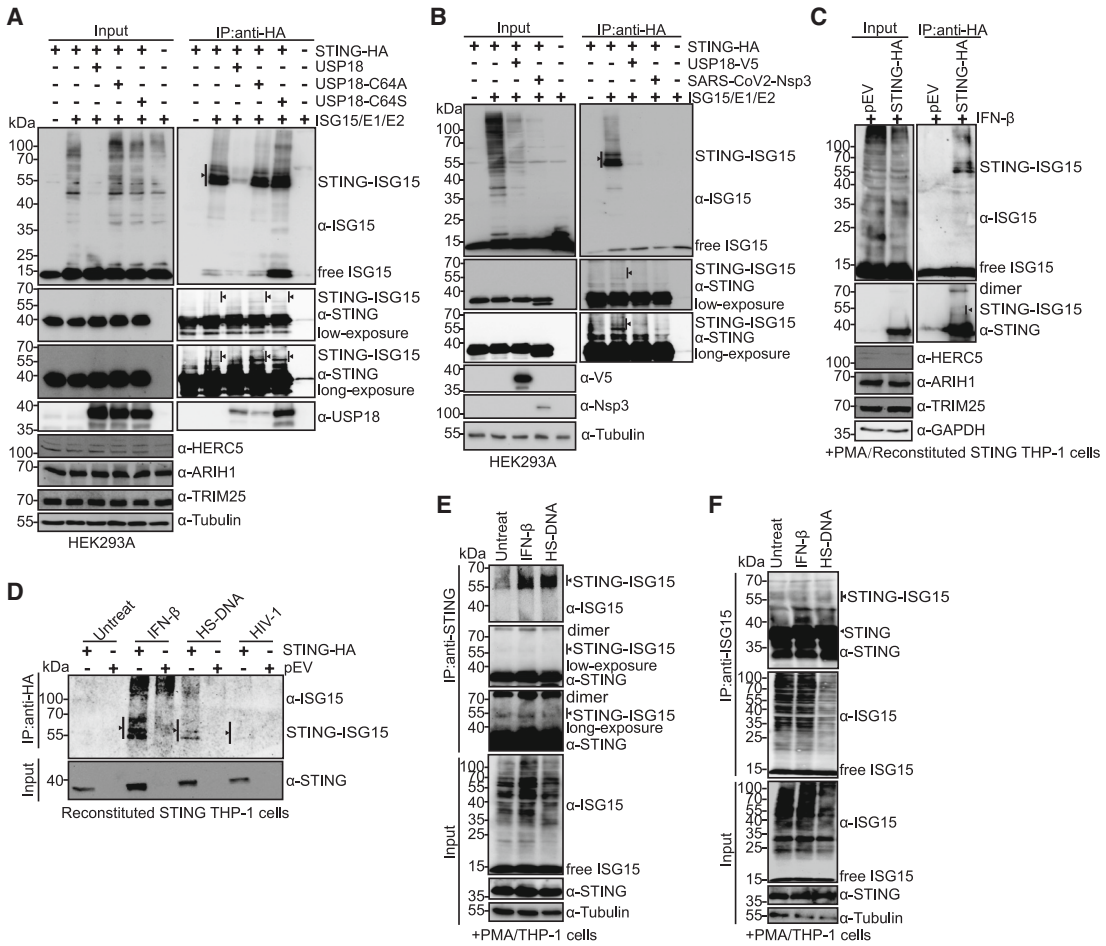

Figure 3. STING is modified by ISG15

(A) Immunoprecipitation (with anti-HA) and immunoblot analysis of STING ISGylation and the expression level of STING-HA, ISG15, USP18, USP18-C64A, USP18-C64S, endogenous HERC5, TRIM25, ARIH1, and tubulin in HEK293A cells that were transfected with indicated plasmids for 48 h.

(B) Immunoprecipitation (with anti-HA) and immunoblot analysis of STING ISGylation and the expression level of STING, ISG15, USP18, SARS-CoV2-Nsp3, and tubulin in HEK293A cells that were transfected with indicated plasmids for 48 h.

(C) Immunoprecipitation (with anti-HA) and immunoblot analysis of STING ISGylation and the expression level of STING, ISG15, endogenous HERC5, TRIM25, ARIH1, and GAPDH in PMA-differentiated reconstituted STING THP-1 cells and lentiviral pLOC empty vector (pEV) control THP-1 cells that were stimulated with 500 U/mL IFN-β for 48 h.

(D) Immunoprecipitation (with anti-HA) and immunoblot analysis of STING ISGylation in reconstituted STING THP-1 cells and pEV control THP-1 cells that were mock treated, stimulated with 500 U/mL IFN-β, transfected with 4 μg/mL HS-DNA, or infected with HIV-1 for 48 h.

(E) Immunoprecipitation (with anti-STING [E] or anti-ISG15 [F]) and immunoblot analysis of STING ISGylation and the expression level of STING, ISG15, and tubulin in PMA-differentiated THP-1 cells that were mock treated, stimulated with 1,000 U/mL IFN-β, or transfected with 4 μg/mL HS-DNA for 48 h. Data are representative of three independent experiments.

K236, K289, K338, K347, and K370) in STING were mutated to arginine (STING-K6R-HA) (Figure 4B). In addition, ISGylation of STING reappeared when single residues in STING-K6R were restored to lysine (Figure 4B). Furthermore, comparing wild-type STING-HA with STING-K6R-HA expressing THP-1 cells, ISGylation was only detectable in wild-type STING (Figure 4C). In line with the HEK293A assay, STING ISGylation was detected in reconstituted STING THP-1 cells upon reintroducing lysines to STING-K6R-HA (Figure 4D). Overall, these data indicate that lysines 224, 236, 289, 338, 347, and 370 are major sites of STING modification by ISG15, and one lysine at these sites is sufficient for robust ISGylation.

K289-linked ISGylation of STING is vital for STING activity

To determine which ISGylation sites regulate STING-induced IFN production, STING or its mutants were co-expressed with ISG15, UBE1L, and UBCH8 in HEK293A cells. Mutation of K289R and K6R of STING, as well as the STING phosphorylation site mutant S366A abolished STING-mediated induction of type I IFN in transfected HEK293A cells comparable to the level of the transfection of wild-type STING (Figure 5A). As expected, this impairment could be restored by replacing R289 to K289 in STING-K6R (Figure 5B). In line with this, type I IFN induction was rescued in STING reconstituted THP-1 cells with STING-K5R-R289K but

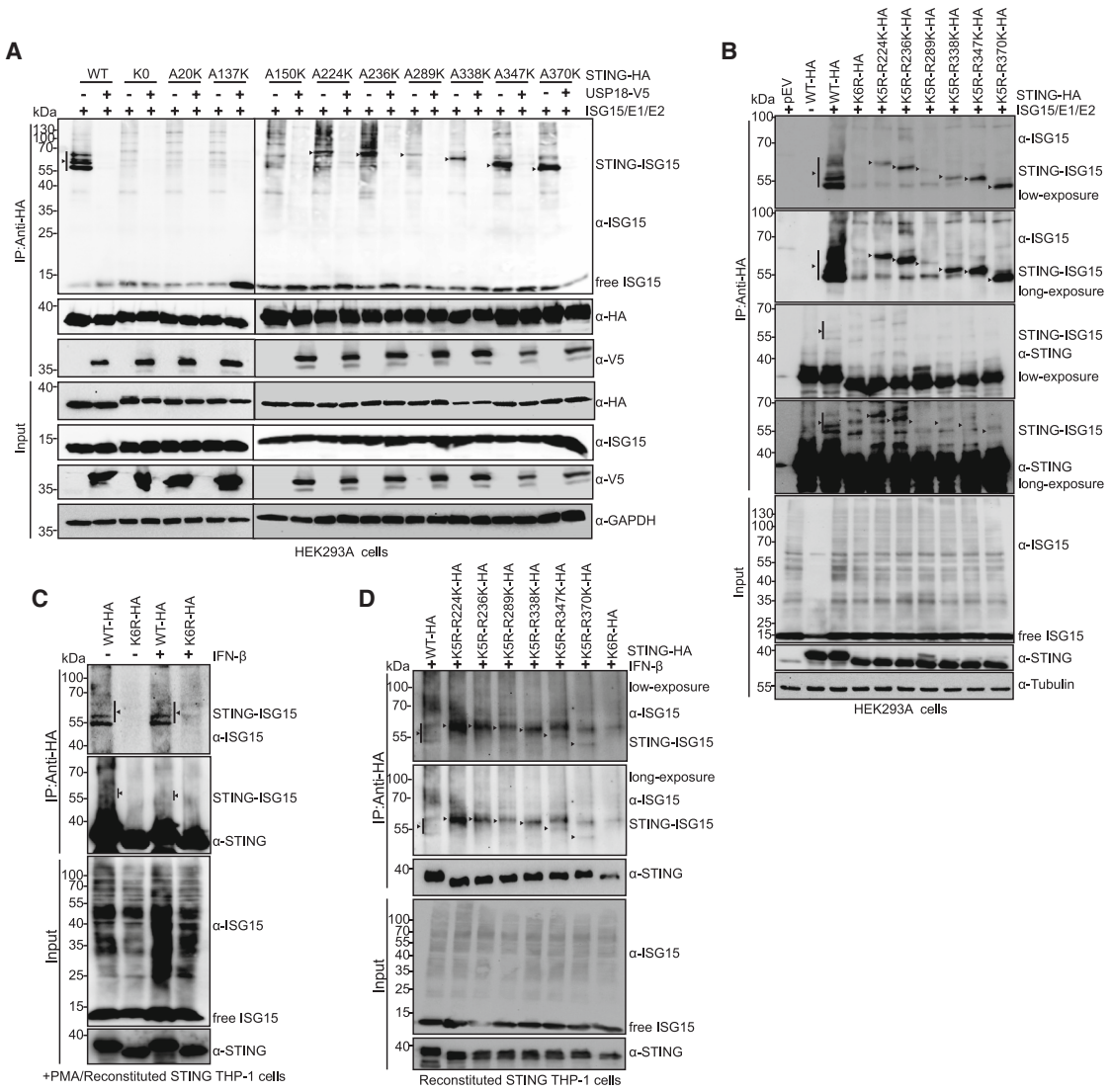

Figure 4. K224, K236, K289, K338, K347, and K370 of STING are modified by ISG15

(A and B) Immunoprecipitation (with anti-HA) and immunoblot analysis of STING ISGylation and the expression level of wild-type or mutant STING-HA, ISG15, USP18-V5, GAPDH, and tubulin in HEK293A cells that were transfected with indicated plasmids for 48 h.

(C) Immunoprecipitation (with anti-HA) and immunoblot analysis of STING ISGylation and the expression level of STING, STING-K6R, ISG15, and tubulin in PMA-differentiated reconstituted STING THP-1 cells that were stimulated with 1,000 U/mL IFN-β for 48 h.

(D) Immunoprecipitation (with anti-HA) and immunoblot analysis of STING ISGylation and the expression level of wild-type or mutant STING, and ISG15 in reconstituted STING THP-1 cells that were stimulated with 500 U/mL IFN-β for 48 h. Data are representative of three independent experiments.

not with the repair of any other arginine residues in STING-K6R after HS-DNA transfection (Figure 5C) and HIV-1 infection (Figure 5D). Furthermore, lower mRNA levels of *IFNB1* and downstream ISGs were detected in STING-K6R and STING-K289R reconstituted STING THP-1 cells (Figure 5E) and transfected HEK293A cells (Figure 5F). To explore the effect of the mutation of STING in response to external stimuli in a physiological genetic and relevant cellular context, we introduced the point mutation K289R into the genomic *STING* locus by CRISPR-Cas9-mediated knockin (KI) in human induced pluripotent stem cells (iPSCs). The iPS system allows differentiation of pluripotent cells into relevant cell types harboring the potential to react upon stimulation. Furthermore, endogenous KI has the advantage of avoiding overexpression artifacts and dysregulated transcription. Therefore, we generated *STING-K289R* mutated cell clones in the apparently healthy human iPSC line PEIi003-A[57] utilizing a gene-editing strategy using CRISPR-Cas9 ribonucleoprotein (RNP) and single-stranded DNA (ssDNA) oligonucleotide introduction by nucleofection. We then identified isogenic cell clones with K289R mutation by sequencing (Figure S1A) and further confirmed the presence of both alleles by biallelic PCR (Figure S1B). The generated iPSC KI-clone PEIi003-A-1 demonstrated a characteristic embryonic stem cell-like (ES-like) phenotype with distinctive cobblestone morphology (Figure S1C). The

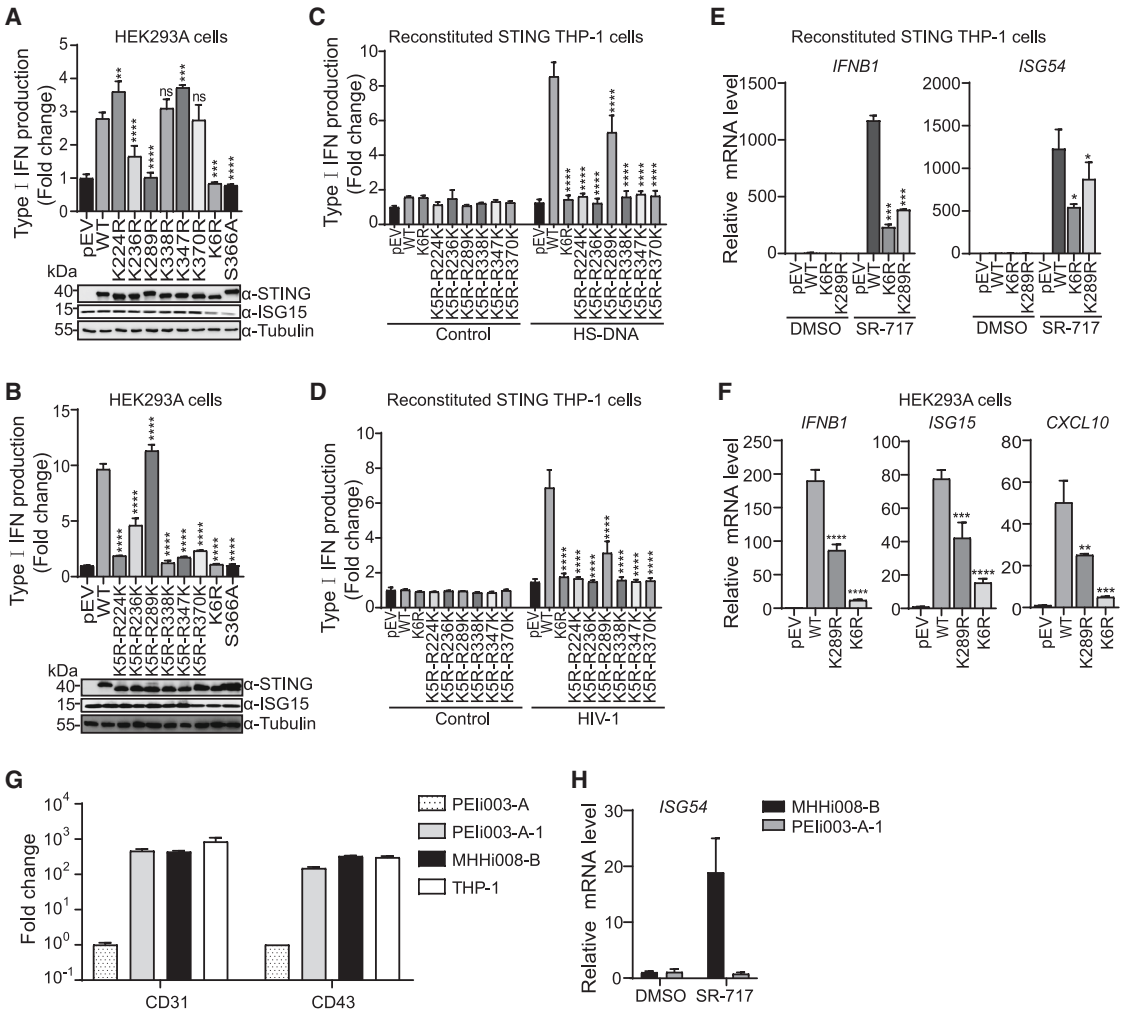

Figure 5. K289 of STING is crucial for IFN induction

(A and B) HEK293A cells were transfected indicated plasmids for 30 h followed by immunoblot analysis and type I interferon production analysis.

(C and D) Undifferentiated reconstituted STING THP-1 cells were transfected with 4 μg/mL HS-DNA (C) or infected with HIV-1 (D) for 48 h followed by type I interferon production analysis.

(E) RT-qPCR analysis of mRNA level of *IFNB1* and *ISG54* in reconstituted STING THP-1 cells that were stimulated with 3.6 μM SR-717 for 2 h. *GAPDH* serves as housekeeping gene.

(F) RT-qPCR analysis of mRNA level of *IFNB1*, *ISG15*, and *CXCL10* in HEK293A cells that were transfected with indicated plasmids for 24 h. *GAPDH* served as housekeeping gene.

(G) RT-qPCR analysis of mRNA level of *CD31* and *CD34* in iPSC-derived hematopoietic progenitor cells from STING-K289R cells PEIi003-A-1 (gray) compared to healthy control cell line MHHi008-B (black). As negative control the parental iPSCs (PEIi003-A) were used and THP-1 cells as a positive control. *RPL13A* served as housekeeping gene.

(H) RT-qPCR analysis of mRNA level of *ISG54* in iPSC-derived hematopoietic progenitor cells that were stimulated with 3.6 μM SR-717 for 24 h. STING-K289R (PEIi003-A-1) cells are shown in gray compared with cells derived from control cell line MHHi008-B in black. *RPL13A* served as housekeeping gene. Significance was determined using one-way ANOVA (Figures 5A–5F) (ns, not significant; *p < 0.05, **p < 0.01, ***p < 0.001, and ****p < 0.0001). Data are representative of three independent experiments (graphs show mean ± SD). See also Figure S1.

pluripotent state was confirmed by immunofluorescence staining of the stem cell markers OCT4 and SOX2 (Figure S1D) as well as RT-qPCR demonstrating elevated expression of *OCT4*, *SOX2*, and *NANOG* relative to human peripheral blood mononuclear cells (PBMCs) (Figure S1E). Further, the generated *STING-K289R*-clone PEIi003-A-1 was capable of differentiation into the germlayer ectoderm, mesoderm, and endoderm (Figure S1F). Next, we differentiated KI PEIi003-A-1 to iPS-derived hematopoietic progenitor cells (HPCs) following the established protocol from Sontag et al.[58] Expression of STING has been verified in HPCs (Figure S1G). Both the control cell line MHHi008-B derived from healthy donor and the *STING-K289R* cell clone possess the ability to differentiate into hematopoietic progenitors verified by expression analysis demonstrating similar level of lineage markers *CD31* and *CD34* (Figure 5G).[59] Interestingly, STING agonist SR-717-induced transcription of *ISG54* was markedly

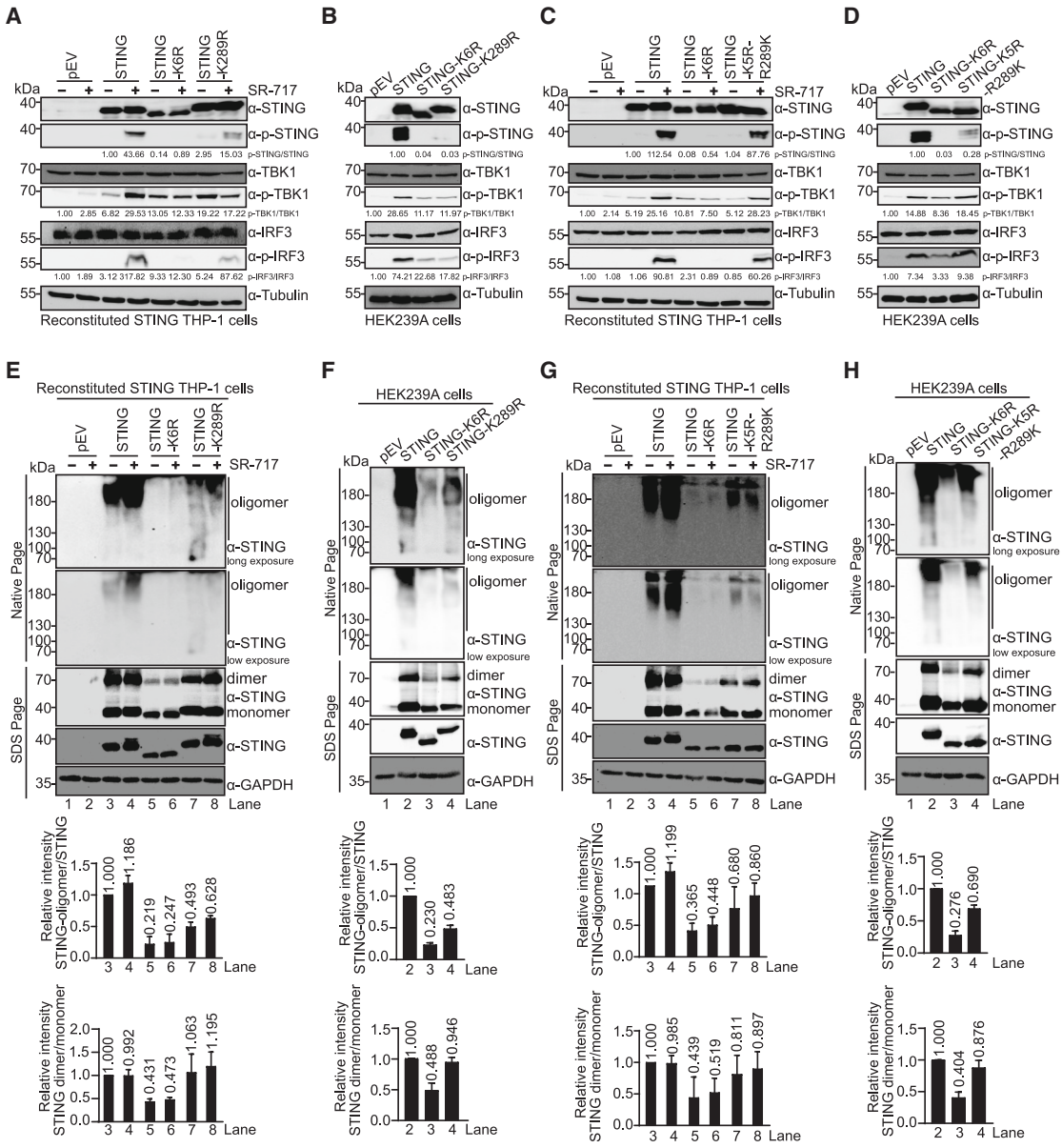

Figure 6. ISGylation of STING facilitates its dimerization and oligomerization

(A–D) Immunoblot analysis of total and phosphorylated STING, TBK1, IRF3, and tubulin in reconstituted STING THP-1 cells that were treated with DMSO or 3.6 μM SR-717 for 2 h (A and C) or in HEK293A cells that were transfected with indicated plasmids for 24 h (B and D).

(E–H) Immunoblot analysis and native immunoblot analysis of STING oligomerization, STING dimerization, STING, and GAPDH in reconstituted STING THP-1 cells that were treated with DMSO or 3.6 μM SR-717 for 2 h (E and G) or in HEK293A cells that were transfected with indicated plasmids for 24 h (F and H). The intensity of p-STING/STING, p-TBK1/TBK1, p-IRF3/IRF3, STING oligomerization, and dimerization were measured with the ImageJ program, and the results are quantifications from multiple independent experiments. Data are representative of three independent experiments (graphs show mean). See also Figure S2.

decreased in *STING-K289R* cells compared to control cells (Figure 5H). Together, these results show that STING lysine 289 is an important ISGylation site required for STING activation.

ISGylation of STING facilitates its dimerization and oligomerization

To understand the consequences of ISGylation, we reconstituted STING knockout THP-1 cells with either STING-K6R or STING-K289R and detected drastically reduced STING agonist-induced phosphorylation of STING, TBK1, and IRF3 compared with cells reconstituted with wild-type STING (Figure 6A). Similarly, we found that transient expression of STING-K6R and STING-K289R in HEK293A cells decreased the phosphorylation level of STING and IRF3 (Figure 6B). In line with our ISGylation data, phosphorylation of STING, TBK1, and IRF3 was partially recovered in

STING-K5R-R289K-expressing cells, but not in STING-K6R cells (Figure 6C). Along these lines, expression of STING-K5R-R289K in HEK293A cells led to robust IRF3 phosphorylation (Figure 6D). This suggests that K289-linked ISGylation regulates STING-mediated activation of the IRF3 pathway. To determine the mechanisms of missing STING activation in the STING mutants, we examined (1) activation of ubiquitination, and (2) dimerization and oligomerization of STING. To test whether the ubiquitination of STING was affected, we co-expressed wild-type or mutant STING together with FLAG-tagged ubiquitin and analyzed STING pull-downs in immunoblots for a ubiquitin signal. Our results show that STING-K6R, STING-K289R, and STING-K5R-R289K had comparable ubiquitination levels to wild-type STING (Figure S2A). This indicates that ubiquitination is not affected by either ISGylation or mutation of ISGylated residues. However, oligomerization of STING-K6R was abrogated in STING agonist-stimulated reconstituted STING THP-1 cells or transfected HEK293A cells (Figures 6E and 6F). In comparison with wild-type STING, the oligomerization of STING-K289R was reduced, whereas the dimerization was similar (Figures 6E and 6F). Next, we examined whether ISGylation of STING-K6R could restore STING oligomerization by mutating K back at residue 289. Importantly, oligomerization of STING was substantially restored in reconstituted STING-K5R-R289K THP-1 cells and transfected HEK293A cells (Figures 6G and 6H). Similarly, the dimerization of STING was partially restored upon introducing R289K in STING-K6R (Figures 6G and 6H). Collectively, these results suggest that ISGylation at K289 promotes its dimerization and facilitates its oligomerization.

STING mutant V155M requires ISGylation for constitutive activity

Gain-of-function mutations in the STING gene lead to a systemic autoinflammatory disease known as SAVI, with STING-V155M being the most prevalent.[60] SAVI patients exhibit a strong transcriptional ISG signature in peripheral whole-blood cells.[20,21] We examined whether ISGylation was required for the activity of the SAVI-STING. Transient expression of wild-type or mutant STING in HEK293A showed that STING-V155M expression induced high levels of type I IFN, STING, and IRF3 phosphorylation, and downstream antiviral gene *ISG15* (Figure 7A). In contrast, the activity of STING-V155M was almost abrogated by mutating K289R or K6R (Figure 7A). We next examined the impact of ISGylation on SAVI-STING in THP-1 cells. We found that STING-V155M-reconstituted THP-1 cells showed type I IFN responses and phosphorylation of STING and IRF3, as well as the induction of ISG15 protein synthesis under unstimulated conditions, whereas SAVI-STING with K289R or K6R lost this activity (Figure 7B). STING-V155M is located at the connector helix loop and is assumed to promote the 180° rotation of the ligand-binding domain, thus resulting in the STING activation irrespective of the presence of cGAMP.[9,61] We examined the oligomerization of STING and showed that STING-V155M with the K289R or K6R mutation significantly reduced oligomerization (Figure 7C). Thus, prevention of STING ISGylation suppressed signaling by constitutively active SAVI-STING.

ISGylation of STING K289 structurally rigidifies the homodimer and leads to additional interactions in oligomers

To assess the structural impact of ISGylation of K289, we created models of the ISGylated STING homodimer, which likely is constitutively minimally ISGylated prior to cGAMP binding, and a dimer of dimers and subjected these to all-atom molecular dynamics (MD) simulations in a membrane environment. Applying constraint network analysis[63] (CNA) on the conformational ensemble of the homodimer revealed that ISGylation of STING structurally rigidifies the STING region involved in the rotation during activation as well as the orthosteric binding site (Figure 7D). This suggests that ISGylation helps conserve a respective STING state. The activated state might be favored particularly as the STING protomers are intertwined in this state making a monomerization less likely. ISGylation furthermore reduces the likelihood of cGAMP binding to the homodimer according to a computed positive cooperative free energy for the allosteric modulation by ISGylation toward cGAMP binding (Equation 1),[62] indicating a negative cooperative effect. The MD simulations of the dimer of dimers reveal additional interactions between two ISG15 linked to neighboring STING (Figures 7E and S3A) in, on average, 71.1% ± 8.4% of the time with an average number of 2.3 ± 0.4 hydrogen bonds (mean ± SEM, n = 20 from 10 replicas and two neighboring moieties per replica) (Figure S3B). Hence, ISGylation can mediate interactions between neighboring STING dimers of dimers and thus might facilitate oligomerization, as suggested by the moderate structural changes within (Figure S3C) and between dimers (Figure S3D). Overall, ISGylation is suggested to stabilize active oligomerized STING by impacting the transformation between states, as cGAMP less likely binds to the ISGylated homodimer, and by forming additional inter-dimer interactions.

DISCUSSION

The activity and stability of STING are regulated by various PTMs to initiate rapid responses against pathogenic DNA while avoiding harmful inflammatory diseases.[22] In this study, we have identified an uncovered PTM of STING that is mediated by ISG15, which promotes its oligomerization and activation under viral infection and DNA challenge, thus enhancing upregulation of downstream type I IFN and inflammatory cytokines. In support of this, we show that (1) ISG15 deficiency inhibits STING-dependent DNA sensing signaling and STING agonist-inducted activation of the antiviral response; (2) STING is ISGylated by ISG15 at K224, K236, K289, K338, K347, and K370 upon viral infection or cytoplasmic DNA challenge; (3) K289-linked ISGylation on STING is essential for STING oligomerization and STING-mediated IFN induction; and (4) repression of ISGylation on STING K289 rescues from the autoimmune phenotypes in STING-SAVI. Collectively, these findings reveal a PTM of STING that promotes both the activation of STING-inducted antiviral immunity and the progression of STING-driven autoimmune disease.

ISG15 is strongly induced by viral infection and type I IFN and is a central player in the host antiviral response through its conjugation to target proteins via ISGylation.[29,30,41] Mass spectrometry-based proteomics studies have identified hundreds of

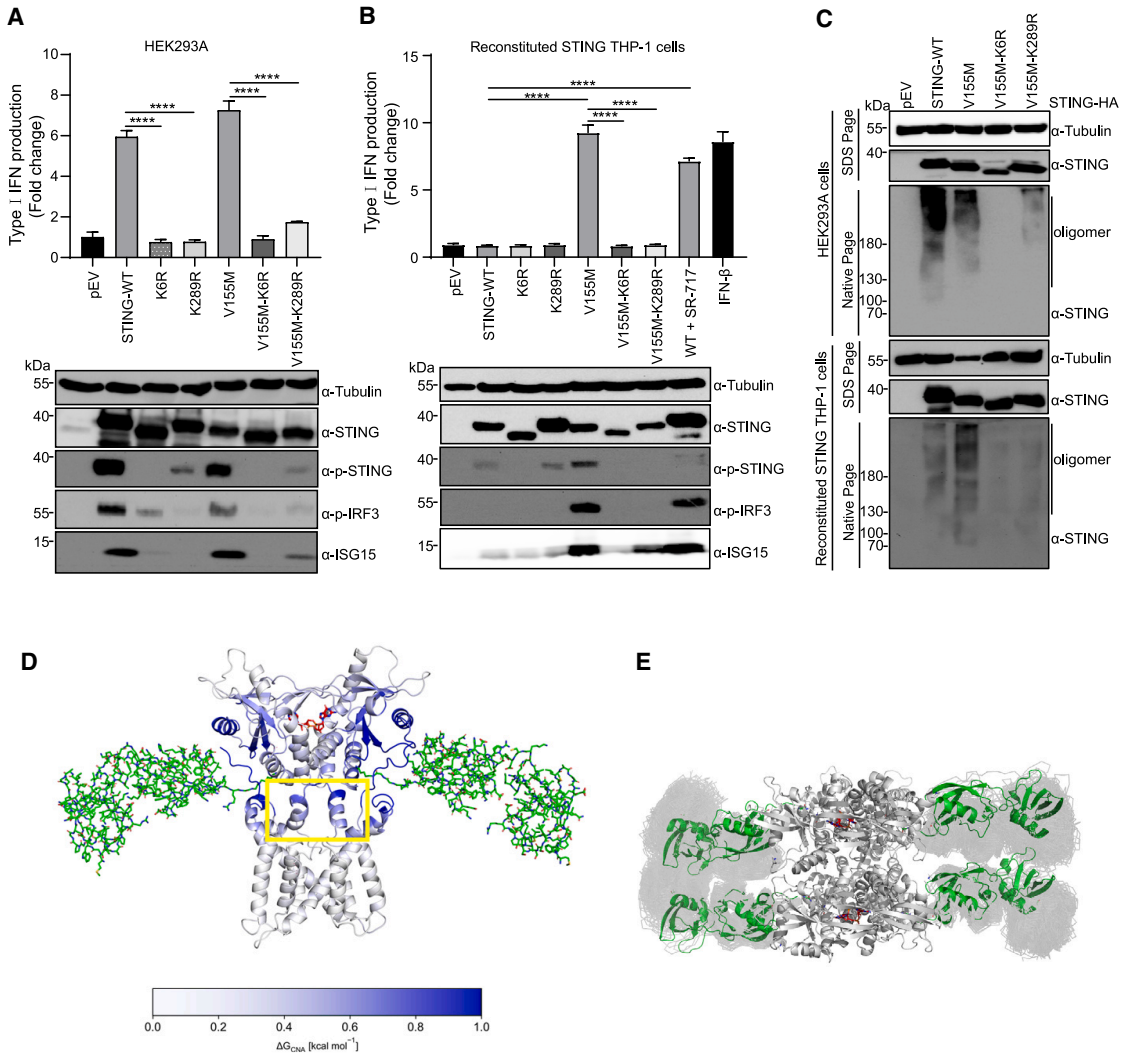

Figure 7. STING mutant V155M requires ISGylation for constitutive activity

(A) HEK293A cells were transfected with indicated plasmids for 30 h followed by immunoblot analysis and type I interferon production analysis.

(B) Reconstituted STING THP-1 cells were stimulated or unstimulated with 3.6 μM SR-717 for 24 h followed by immunoblot analysis and type I interferon production analysis.

(C) Reconstituted STING THP-1 cells or HEK293A cells were transfected with indicated plasmids for 24 h, followed by immunoblot analysis and native immunoblot analysis. Significance was determined using one-way ANOVA and two-tailed Student's t test (Figures 7A and 7B) (*$p < 0.05$, **$p < 0.01$, ***$p < 0.001$, and ****$p < 0.0001$).

(D) Changes in the structural rigidity of STING ($\Delta G_{i,CNA}$) due to ISGylation (green) as predicted by CNA[62] mapped (blue gradient) on a per-residue basis onto the cGAMP-bound (red sticks) homodimer of STING. ISGylation rigidifies the region (yellow box) responsible for the rotation upon activation of STING and the orthosteric binding site.

(E) Top view of the conformational space sampled by ISG15 (dark gray ribbons) attached to an STING dimer of dimers (gray cartoon) during an MD simulation in relation to the initial conformation of ISG15 (green cartoon). ISG15 in neighboring STING pairs contact each other (see also Figures S3A and S3B). Data are representative of three independent experiments (graphs show mean ± SD) or 10 independent replicas of MD simulations.

host proteins that are ISGylated and only a few proteins have been investigated.[64–66] For example, the ISGylation of IRF3 prevents the proteasomal degradation of IRF3 and enhances the intracellular IFN response upon viral infection.[44] ISGylation of phosphorylated signal transducer and activator of transcription 1 (STAT1) inhibited its polyubiquitylation and subsequent degradation.[67] Recently, ISGylation of MDA5 and cGAS were described to be essential for viral infection-induced innate immune response.[46,47] However, key ISGylated targets in the host remain largely unknown. In this study, we demonstrated that STING needs to be ISGylated upon cytosolic DNA stimulation and to promote IFN-mediated defense in the context of HIV-1 infection. However, it seems that only a small fraction of the total STING is modified by ISG15, thus it is still a challenge to understand how ISGylation affects the overall function of STING. It is possible that ISGylation on STING is sufficient to promote larger assemblies of

STING protein polymers, similar to the situation for cGAS.[47] We observed that co-expression of STING and USP18-C64S resulted in enhanced STING ISGylation and detectable free ISG15 in the IP sample (Figure 3A), which is likely caused by the increased stability of the STING-USP18-C64S complex (Figure 3A) and an enhanced binding of free ISG15 to USP18-C64S compared with wild-type USP18.[56]

We have provided several lines of evidence that multiple lysine residues of STING can be modified by ISG15 under cytosolic DNA challenge. STING harbors six ISG15 attachment sites: K224, K236, K289, K338, K347, and K370. Significantly, K289-linked ISGylation of STING is essential for STING activity. In contrast, replacing R289K in STING-K6R recovered the oligomerization and substantially enhanced the activity of STING in cells after HIV-1 infection or in the presence of cytoplasmic DNA. Furthermore, we validated the impact of the K289 site in a physiological genetic and relevant cellular context by generating an endogenous mutation of STING at K289 by CRISPR-Cas9 KI in human iPSCs and found that *STING-K289R* mutation impaired STING agonist SR-717-induced transcription of the *ISG54* gene compared with control cells. These findings suggest that ISGylation at K289 of STING is vital for STING-dependent innate immune signaling.

STING signaling is dynamically regulated by polyubiquitination and relies on different types of polyubiquitin chains at one or multiple lysine residues involving E3 ligases TRIM32, AMFR, and ring finger protein 115 (RNF115).[22] TRIM32 targets STING for K63-linked polyubiquitination at residues K20, K150, K224, and K236, while AMFR targets STING for K27-linked polyubiquitination at K137, K150, K224, and K236 to facilitate TBK1 recruitment and activation.[24,25] In addition, STING can be ubiquitinated by K63-linked polyubiquitination mediated by the E3 ligase RNF115 at K20, K224, and K289, which enhances the aggregation of STING and promotes the recruitment of TBK1 after viral infection.[68] Mutation of STING at K20, K224, or K289 into arginine residues impaired RNF115-mediated ubiquitination and abolished its dimerization and aggregation.[68] In contrast, we demonstrated that mutation of STING-K6R or STING-K289R inhibits oligomer formation but not ubiquitination. These results suggest that multiple lysine-mediated ubiquitination modifications collectively regulate the function of STING, that STING is efficiently ubiquitylated at K20, K137, or K150, which were not changed in STING-K6R. It will be a task for the future to describe the dynamics of diverse modifications at single lysines and their impact on STING function.

Liu et al. showed that endogenous STING can form oligomers in both resting and active states, and cGAMP treatment enhances the levels of these higher-order oligomers.[10] Based on this model, autoinhibited STING forms oligomers with bilayer assembly zippering two ER membranes, whereas the activated STING forms a curved monolayer filament that deforms the membrane to support its ER exit.[10] We reconstituted STING-depleted THP-1 cells with WT-STING or STING mutants and found that STING-K289R and STING-K6R abrogated its oligomerization without cGAMP treatment, whereas STING-K5R-R289K partially rescued the levels of oligomers, compared with wild-type STING. Our data suggest that loss of ISGylation on STING inhibits its oligomer formation and activation. The natural mutation V155M in human STING can cause severe SAVI disease.[20,21,69] Patients with SAVI, have constitutively activated STING, leading to increased release of inflammatory cytokines and IFNs.[20,21,69] Mechanistically, STING-V155M localizes to perinuclear compartments, not the ER, with a 180° rotation of the ligand-binding domain along a connector helix loop of STING in a cGAMP-independent manner.[9,21,69] Our results showed that transient STING-V155M expression in HEK293A cells or unstimulated-STING-V155M reconstituted THP-1 cells upregulated the activation of STING, IRF3, and the expression of the downstream gene of ISG15. In contrast, the K289R or K6R mutation of STING-V155M prevents the oligomer formation, resulting in the inhibition of IRF3 activation and IFN induction, suggesting that loss of ISGylation inhibits oligomerization and activation of STING. Thus, suppression of ISGylation could inhibit a gain-of-function phenotype in SAVI-STING. Understanding how ISGylation of STING at K289 regulates STING oligomerization and activation depends on a more detailed structural and functional analysis of full-length STING.

Our molecular modeling suggests that ISGylation of the homodimer rigidifies the region responsible for the rotation upon activation and thus might foster the conservation of the activated state as well as that cGAMP less likely binds to the ISGylated homodimer. ISGylation furthermore leads to enhanced interactions in STING dimers of dimers. Together, this suggests that ISGylation favors the activated oligomerized state of STING.

In summary, we propose a regulatory mechanism of STING by ISGylation in innate immune activation and inflammatory diseases. These findings open perspectives to uncover the enigmatic aspects of activation of STING-mediated viral restriction and to treat STING-mediated inflammatory diseases by suppressing the ISGylation of STING.

Limitations of the study

Our study suggests that ISGylation of STING at K289 is important for its activation. Although we demonstrated that STING oligomerization is decreased if ISGylation is blocked, our experiments do not allow conclusions regarding cGAMP binding, conformational changes in STING pre or post cGAMP binding, or a direct regulation of subsequent STING oligomer formation or stability. However, molecular modeling suggests that ISGylation of K289 is an important regulator of oligomerization. Furthermore, we cannot exclude that ISGylation is important for the COPII vesicle transport of activated STING or any subsequent steps.

To dissect the molecular mechanism of STING ISGylation in regulating the production of type I interferon, we relied on diverse *in vitro* human cell-based assays and human iPS cell models to approach the physiological setting using an STING knockin K289R. However, the impact of STING ISGylation on interferon regulation and HIV-1 replication *in vivo* remains to be examined in future studies. Moreover, ISG15 from humans and mice differ, and thus ISGylation regulation may be different.[70]

STAR★METHODS

Detailed methods are provided in the online version of this paper and include the following:

- KEY RESOURCES TABLE

SUPPLEMENTAL INFORMATION

Supplemental information can be found online at https://doi.org/10.1016/j.celrep.2023.113277.

ACKNOWLEDGMENTS

We thank Wioletta Hörschken, Christiane Tondera, Janna Lustig, and Heike Schmitz for their excellent technical assistance. We also thank Björn Stork, David Schlütermann, Karl Lang, Klaus Harbers, Klaus-Peter Knobeloch, Nathaniel R. Landau, Oya Cingöz, and Veit Hornung for reagents. The following reagent was obtained from Didier Trono through the NIH AIDS Reagent Program, Division of AIDS, NIAID, NIH: psPAX2 (catalog number 11348). We thank Dieter Häussinger and Sander Smits for support and discussion.

C.M. is supported by the Heinz-Ansmann Foundation for AIDS Research and Dr. Friedhelm Haak. This work was supported by Deutsche Forschungsgemeinschaft (DFG): SPP1923 project MU 1608/9-2 to C.M. and SPP1923 project KO 4573/1-2 to R.K. C.L. is supported by China Scholarship Council (202008080281). K.M.J.S. was supported by the DFG (SPP1923, SP1600/7-1) and the German Ministry for Education and Research (BMBF, project IMMUNOMOD). DFG project 452147069 DR 632/2-1 to I.D., RTG 1949/2 project TP01 to I.D. The Center for Structural Studies is funded by the DFG (Grant number 417919780). We are grateful for computational support and infrastructure provided by the "Zentrum für Informations-und Medientechnologie" (ZIM) at the Heinrich Heine University Düsseldorf and for computational resources provided by the John von Neumann Institute for Computing (NIC) to H.G. on the supercomputer JUWELS at the Jülich Supercomputing Center (JSC) (user-IDs: HKF7, VSK33).

AUTHOR CONTRIBUTIONS

Conceptualization, C.L. and C.M.; methodology, C.L., E.O.K., N.V.F., H.G, R.K., and C.M.; investigation, C.L., E.O.K., N.V.F., X.T., J.L., C.G.W.G., and C.M.; writing – original draft, C.L. and N.V.F.; writing – review & editing, C.L., E.O.K., M.H., H.G., B.G., I.D., K.M.J.S., P.A.L., T.L., R.K., and C.M.; funding acquisition, C.L., R.K., and C.M.; resources, O.M., A.H., U.M., R.T., T.K., H.C.X., P.A.L., and I.D.; supervision, R.K. and C.M.

DECLARATION OF INTERESTS

The authors declare no competing interests.

INCLUSION AND DIVERSITY

We support inclusive, diverse, and equitable conduct of research.

Received: May 4, 2023
Revised: September 6, 2023
Accepted: September 28, 2023

REFERENCES

1. Turvey, S.E., and Broide, D.H. (2010). Innate immunity. J. Allergy Clin. Immunol. *125*, S24–S32. https://doi.org/10.1016/j.jaci.2009.07.016.
2. Akira, S., Uematsu, S., and Takeuchi, O. (2006). Pathogen recognition and innate immunity. Cell *124*, 783–801. https://doi.org/10.1016/j.cell.2006.02.015.
3. Bartok, E., and Hartmann, G. (2020). Immune Sensing Mechanisms that Discriminate Self from Altered Self and Foreign Nucleic Acids. Immunity *53*, 54–77. https://doi.org/10.1016/j.immuni.2020.06.014.
4. Liu, G., and Gack, M.U. (2020). Distinct and Orchestrated Functions of RNA Sensors in Innate Immunity. Immunity *53*, 26–42. https://doi.org/10.1016/j.immuni.2020.03.017.
5. Sun, L., Wu, J., Du, F., Chen, X., and Chen, Z.J. (2013). Cyclic GMP-AMP synthase is a cytosolic DNA sensor that activates the type I interferon pathway. Science *339*, 786–791. https://doi.org/10.1126/science.1232458.
6. Wu, J., Sun, L., Chen, X., Du, F., Shi, H., Chen, C., and Chen, Z.J. (2013). Cyclic GMP-AMP is an endogenous second messenger in innate immune signaling by cytosolic DNA. Science *339*, 826–830. https://doi.org/10.1126/science.1229963.
7. Hopfner, K.P., and Hornung, V. (2020). Molecular mechanisms and cellular functions of cGAS-STING signalling. Nat. Rev. Mol. Cell Biol. *21*, 501–521. https://doi.org/10.1038/s41580-020-0244-x.
8. Ishikawa, H., and Barber, G.N. (2008). STING is an endoplasmic reticulum adaptor that facilitates innate immune signalling. Nature *455*, 674–678. https://doi.org/10.1038/nature07317.
9. Shang, G., Zhang, C., Chen, Z.J., Bai, X.C., and Zhang, X. (2019). Cryo-EM structures of STING reveal its mechanism of activation by cyclic GMP-AMP. Nature *567*, 389–393. https://doi.org/10.1038/s41586-019-0998-5.
10. Liu, S., Yang, B., Hou, Y., Cui, K., Yang, X., Li, X., Chen, L., Liu, S., Zhang, Z., Jia, Y., et al. (2023). The mechanism of STING autoinhibition and activation. Mol. Cell *83*, 1502–1518.e10. https://doi.org/10.1016/j.molcel.2023.03.029.
11. Ergun, S.L., Fernandez, D., Weiss, T.M., and Li, L. (2019). STING Polymer Structure Reveals Mechanisms for Activation, Hyperactivation, and Inhibition. Cell *178*, 290–301.e10. https://doi.org/10.1016/j.cell.2019.05.036.
12. Zhang, C., Shang, G., Gui, X., Zhang, X., Bai, X.C., and Chen, Z.J. (2019). Structural basis of STING binding with and phosphorylation by TBK1. Nature *567*, 394–398. https://doi.org/10.1038/s41586-019-1000-2.
13. Balka, K.R., Louis, C., Saunders, T.L., Smith, A.M., Calleja, D.J., D'Silva, D.B., Moghaddas, F., Tailler, M., Lawlor, K.E., Zhan, Y., et al. (2020). TBK1 and IKKepsilon Act Redundantly to Mediate STING-Induced NF-kappaB Responses in Myeloid Cells. Cell Rep. *31*, 107492. https://doi.org/10.1016/j.celrep.2020.03.056.
14. Yum, S., Li, M., Fang, Y., and Chen, Z.J. (2021). TBK1 recruitment to STING activates both IRF3 and NF-kappaB that mediate immune defense against tumors and viral infections. Proc. Natl. Acad. Sci. USA *118*, e2100225118. https://doi.org/10.1073/pnas.2100225118.
15. Tanaka, Y., and Chen, Z.J. (2012). STING specifies IRF3 phosphorylation by TBK1 in the cytosolic DNA signaling pathway. Sci. Signal. *5*, ra20. https://doi.org/10.1126/scisignal.2002521.

16. Mankan, A.K., Schmidt, T., Chauhan, D., Goldeck, M., Höning, K., Gaidt, M., Kubarenko, A.V., Andreeva, L., Hopfner, K.P., and Hornung, V. (2014). Cytosolic RNA:DNA hybrids activate the cGAS-STING axis. EMBO J. *33*, 2937–2946. https://doi.org/10.15252/embj.201488726.

17. Barnowski, C., Ciupka, G., Tao, R., Jin, L., Busch, D.H., Tao, S., and Drexler, I. (2020). Efficient Induction of Cytotoxic T Cells by Viral Vector Vaccination Requires STING-Dependent DC Functions. Front. Immunol. *11*, 1458. https://doi.org/10.3389/fimmu.2020.01458.

18. Reinert, L.S., Lopušná, K., Winther, H., Sun, C., Thomsen, M.K., Nandakumar, R., Mogensen, T.H., Meyer, M., Vægter, C., Nyengaard, J.R., et al. (2016). Sensing of HSV-1 by the cGAS-STING pathway in microglia orchestrates antiviral defence in the CNS. Nat. Commun. *7*, 13348. https://doi.org/10.1038/ncomms13348.

19. Li, Y., Wilson, H.L., and Kiss-Toth, E. (2017). Regulating STING in health and disease. J. Inflamm. *14*, 11. https://doi.org/10.1186/s12950-017-0159-2.

20. Fremond, M.L., Hadchouel, A., Berteloot, L., Melki, I., Bresson, V., Barnabei, L., Jeremiah, N., Belot, A., Bondet, V., Brocq, O., et al. (2021). Overview of STING-Associated Vasculopathy with Onset in Infancy (SAVI) Among 21 Patients. J. Allergy Clin. Immunol. Pract. *9*, 803–818.e811. https://doi.org/10.1016/j.jaip.2020.11.007.

21. Wang, Y., Wang, F., and Zhang, X. (2021). STING-associated vasculopathy with onset in infancy: a familial case series report and literature review. Ann. Transl. Med. *9*, 176. https://doi.org/10.21037/atm-20-6198.

22. Kang, J., Wu, J., Liu, Q., Wu, X., Zhao, Y., and Ren, J. (2022). Post-Translational Modifications of STING: A Potential Therapeutic Target. Front. Immunol. *13*, 888147. https://doi.org/10.3389/fimmu.2022.888147.

23. Tsuchida, T., Zou, J., Saitoh, T., Kumar, H., Abe, T., Matsuura, Y., Kawai, T., and Akira, S. (2010). The ubiquitin ligase TRIM56 regulates innate immune responses to intracellular double-stranded DNA. Immunity *33*, 765–776. https://doi.org/10.1016/j.immuni.2010.10.013.

24. Wang, Q., Liu, X., Cui, Y., Tang, Y., Chen, W., Li, S., Yu, H., Pan, Y., and Wang, C. (2014). The E3 ubiquitin ligase AMFR and INSIG1 bridge the activation of TBK1 kinase by modifying the adaptor STING. Immunity *41*, 919–933. https://doi.org/10.1016/j.immuni.2014.11.011.

25. Zhang, J., Hu, M.M., Wang, Y.Y., and Shu, H.B. (2012). TRIM32 protein modulates type I interferon induction and cellular antiviral response by targeting MITA/STING protein for K63-linked ubiquitination. J. Biol. Chem. *287*, 28646–28655. https://doi.org/10.1074/jbc.M112.362608.

26. Kong, L., Sui, C., Chen, T., Zhang, L., Zhao, W., Zheng, Y., Liu, B., Cheng, X., and Gao, C. (2023). The ubiquitin E3 ligase TRIM10 promotes STING aggregation and activation in the Golgi apparatus. Cell Rep. *42*, 112306. https://doi.org/10.1016/j.celrep.2023.112306.

27. Hu, M.M., Yang, Q., Xie, X.Q., Liao, C.Y., Lin, H., Liu, T.T., Yin, L., and Shu, H.B. (2016). Sumoylation Promotes the Stability of the DNA Sensor cGAS and the Adaptor STING to Regulate the Kinetics of Response to DNA Virus. Immunity *45*, 555–569. https://doi.org/10.1016/j.immuni.2016.08.014.

28. Mukai, K., Konno, H., Akiba, T., Uemura, T., Waguri, S., Kobayashi, T., Barber, G.N., Arai, H., and Taguchi, T. (2016). Activation of STING requires palmitoylation at the Golgi. Nat. Commun. *7*, 11932. https://doi.org/10.1038/ncomms11932.

29. Haas, A.L., Ahrens, P., Bright, P.M., and Ankel, H. (1987). Interferon induces a 15-kilodalton protein exhibiting marked homology to ubiquitin. J. Biol. Chem. *262*, 11315–11323.

30. Loeb, K.R., and Haas, A.L. (1992). The interferon-inducible 15-kDa ubiquitin homolog conjugates to intracellular proteins. J. Biol. Chem. *267*, 7806–7813.

31. Dastur, A., Beaudenon, S., Kelley, M., Krug, R.M., and Huibregtse, J.M. (2006). Herc5, an interferon-induced HECT E3 enzyme, is required for conjugation of ISG15 in human cells. J. Biol. Chem. *281*, 4334–4338. https://doi.org/10.1074/jbc.M512830200.

32. Kim, K.I., Giannakopoulos, N.V., Virgin, H.W., and Zhang, D.E. (2004). Interferon-inducible ubiquitin E2, Ubc8, is a conjugating enzyme for protein ISGylation. Mol. Cell Biol. *24*, 9592–9600. https://doi.org/10.1128/MCB.24.21.9592-9600.2004.

33. Okumura, F., Zou, W., and Zhang, D.E. (2007). ISG15 modification of the eIF4E cognate 4EHP enhances cap structure-binding activity of 4EHP. Genes Dev. *21*, 255–260. https://doi.org/10.1101/gad.1521607.

34. Wong, J.J.Y., Pung, Y.F., Sze, N.S.K., and Chin, K.C. (2006). HERC5 is an IFN-induced HECT-type E3 protein ligase that mediates type I IFN-induced ISGylation of protein targets. Proc. Natl. Acad. Sci. USA *103*, 10735–10740. https://doi.org/10.1073/pnas.0600397103.

35. Yuan, W., and Krug, R.M. (2001). Influenza B virus NS1 protein inhibits conjugation of the interferon (IFN)-induced ubiquitin-like ISG15 protein. EMBO J. *20*, 362–371. https://doi.org/10.1093/emboj/20.3.362.

36. Zhao, C., Beaudenon, S.L., Kelley, M.L., Waddell, M.B., Yuan, W., Schulman, B.A., Huibregtse, J.M., and Krug, R.M. (2004). The UbcH8 ubiquitin E2 enzyme is also the E2 enzyme for ISG15, an IFN-alpha/beta-induced ubiquitin-like protein. Proc. Natl. Acad. Sci. USA *101*, 7578–7582. https://doi.org/10.1073/pnas.0402528101.

37. Zou, W., and Zhang, D.E. (2006). The interferon-inducible ubiquitin-protein isopeptide ligase (E3) EFP also functions as an ISG15 E3 ligase. J. Biol. Chem. *281*, 3989–3994. https://doi.org/10.1074/jbc.M510787200.

38. Jiménez Fernández, D., Hess, S., and Knobeloch, K.P. (2019). Strategies to Target ISG15 and USP18 Toward Therapeutic Applications. Front. Chem. *7*, 923. https://doi.org/10.3389/fchem.2019.00923.

39. Lenschow, D.J., Lai, C., Frias-Staheli, N., Giannakopoulos, N.V., Lutz, A., Wolff, T., Osiak, A., Levine, B., Schmidt, R.E., García-Sastre, A., et al. (2007). IFN-stimulated gene 15 functions as a critical antiviral molecule against influenza, herpes, and Sindbis viruses. Proc. Natl. Acad. Sci. USA *104*, 1371–1376. https://doi.org/10.1073/pnas.0607038104.

40. Lai, C., Struckhoff, J.J., Schneider, J., Martinez-Sobrido, L., Wolff, T., García-Sastre, A., Zhang, D.E., and Lenschow, D.J. (2009). Mice lacking the ISG15 E1 enzyme UbE1L demonstrate increased susceptibility to both mouse-adapted and non-mouse-adapted influenza B virus infection. J. Virol. *83*, 1147–1151. https://doi.org/10.1128/JVI.00105-08.

41. Perng, Y.C., and Lenschow, D.J. (2018). ISG15 in antiviral immunity and beyond. Nat. Rev. Microbiol. *16*, 423–439. https://doi.org/10.1038/s41579-018-0020-5.

42. Durfee, L.A., Lyon, N., Seo, K., and Huibregtse, J.M. (2010). The ISG15 conjugation system broadly targets newly synthesized proteins: implications for the antiviral function of ISG15. Mol. Cell *38*, 722–732. https://doi.org/10.1016/j.molcel.2010.05.002.

43. Okumura, A., Lu, G., Pitha-Rowe, I., and Pitha, P.M. (2006). Innate antiviral response targets HIV-1 release by the induction of ubiquitin-like protein ISG15. Proc. Natl. Acad. Sci. USA *103*, 1440–1445. https://doi.org/10.1073/pnas.0510518103.

44. Shi, H.X., Yang, K., Liu, X., Liu, X.Y., Wei, B., Shan, Y.F., Zhu, L.H., and Wang, C. (2010). Positive regulation of interferon regulatory factor 3 activation by Herc5 via ISG15 modification. Mol. Cell Biol. *30*, 2424–2436. https://doi.org/10.1128/MCB.01466-09.

45. Kim, M.J., Hwang, S.Y., Imaizumi, T., and Yoo, J.Y. (2008). Negative feedback regulation of RIG-I-mediated antiviral signaling by interferon-induced ISG15 conjugation. J. Virol. *82*, 1474–1483. https://doi.org/10.1128/JVI.01650-07.

46. Liu, G., Lee, J.H., Parker, Z.M., Acharya, D., Chiang, J.J., van Gent, M., Riedl, W., Davis-Gardner, M.E., Wies, E., Chiang, C., and Gack, M.U. (2021). ISG15-dependent activation of the sensor MDA5 is antagonized by the SARS-CoV-2 papain-like protease to evade host innate immunity. Nat. Microbiol. *6*, 467–478. https://doi.org/10.1038/s41564-021-00884-1.

47. Xiong, T.C., Wei, M.C., Li, F.X., Shi, M., Gan, H., Tang, Z., Dong, H.P., Liuyu, T., Gao, P., Zhong, B., et al. (2022). The E3 ubiquitin ligase ARIH1 promotes antiviral immunity and autoimmunity by inducing mono-ISGylation and oligomerization of cGAS. Nat. Commun. *13*, 5973. https://doi.org/10.1038/s41467-022-33671-5.

48. Malakhov, M.P., Malakhova, O.A., Kim, K.I., Ritchie, K.J., and Zhang, D.E. (2002). UBP43 (USP18) specifically removes ISG15 from conjugated proteins. J. Biol. Chem. *277*, 9976–9981. https://doi.org/10.1074/jbc.M109078200.

49. Shin, D., Mukherjee, R., Grewe, D., Bojkova, D., Baek, K., Bhattacharya, A., Schulz, L., Widera, M., Mehdipour, A.R., Tascher, G., et al. (2020). Papain-like protease regulates SARS-CoV-2 viral spread and innate immunity. Nature *587*, 657–662. https://doi.org/10.1038/s41586-020-2601-5.

50. Osei Kuffour, E., König, R., Häussinger, D., Schulz, W.A., and Münk, C. (2019). ISG15 Deficiency Enhances HIV-1 Infection by Accumulating Misfolded p53. mBio *10*, 013422–e1419. https://doi.org/10.1128/mBio.01342-19.

51. Navarro, L., Mowen, K., Rodems, S., Weaver, B., Reich, N., Spector, D., and David, M. (1998). Cytomegalovirus activates interferon immediate-early response gene expression and an interferon regulatory factor 3-containing interferon-stimulated response element-binding complex. Mol. Cell Biol. *18*, 3796–3802. https://doi.org/10.1128/MCB.18.7.3796.

52. Gao, D., Wu, J., Wu, Y.T., Du, F., Aroh, C., Yan, N., Sun, L., and Chen, Z.J. (2013). Cyclic GMP-AMP synthase is an innate immune sensor of HIV and other retroviruses. Science *341*, 903–906. https://doi.org/10.1126/science.1240933.

53. Yin, X., Langer, S., Zhang, Z., Herbert, K.M., Yoh, S., Konig, R., and Chanda, S.K. (2020). Sensor Sensibility-HIV-1 and the Innate Immune Response. Cells *9*. https://doi.org/10.3390/cells9010254.

54. Chin, E.N., Yu, C., Vartabedian, V.F., Jia, Y., Kumar, M., Gamo, A.M., Vernier, W., Ali, S.H., Kissai, M., Lazar, D.C., et al. (2020). Antitumor activity of a systemic STING-activating non-nucleotide cGAMP mimetic. Science *369*, 993–999. https://doi.org/10.1126/science.abb4255.

55. Li, M., Ferretti, M., Ying, B., Descamps, H., Lee, E., Dittmar, M., Lee, J.S., Whig, K., Kamalia, B., Dohnalová, L., et al. (2021). Pharmacological activation of STING blocks SARS-CoV-2 infection. Sci. Immunol. *6*, eabi9007. https://doi.org/10.1126/sciimmunol.abi9007.

56. Vuillier, F., Li, Z., Commere, P.H., Dynesen, L.T., and Pellegrini, S. (2019). USP18 and ISG15 coordinately impact on SKP2 and cell cycle progression. Sci. Rep. *9*, 4066. https://doi.org/10.1038/s41598-019-39343-7.

57. Fuchs, N.V., Schieck, M., Neuenkirch, M., Tondera, C., Schmitz, H., Steinemann, D., Göhring, G., and König, R. (2020). Induced pluripotent stem cell line (PEIi003-A) derived from an apparently healthy male individual. Stem Cell Res. *42*, 101679. https://doi.org/10.1016/j.scr.2019.101679.

58. Sontag, S., Förster, M., Qin, J., Wanek, P., Mitzka, S., Schüler, H.M., Koschmieder, S., Rose-John, S., Seré, K., and Zenke, M. (2017). Modelling IRF8 Deficient Human Hematopoiesis and Dendritic Cell Development with Engineered iPS Cells. Stem Cell. *35*, 898–908. https://doi.org/10.1002/stem.2565.

59. Haase, A., Glienke, W., Engels, L., Göhring, G., Esser, R., Arseniev, L., and Martin, U. (2019). GMP-compatible manufacturing of three iPS cell lines from human peripheral blood. Stem Cell Res. *35*, 101394. https://doi.org/10.1016/j.scr.2019.101394.

60. Frémond, M.L., and Crow, Y.J. (2021). STING-Mediated Lung Inflammation and Beyond. J. Clin. Immunol. *41*, 501–514. https://doi.org/10.1007/s10875-021-00974-z.

61. Lin, B., Berard, R., Al Rasheed, A., Aladba, B., Kranzusch, P.J., Henderlight, M., Grom, A., Kahle, D., Torreggiani, S., Aue, A.G., et al. (2020). A novel STING1 variant causes a recessive form of STING-associated vasculopathy with onset in infancy (SAVI). J. Allergy Clin. Immunol. *146*, 1204–1208.e6. https://doi.org/10.1016/j.jaci.2020.06.032.

62. Pfleger, C., Minges, A., Boehm, M., McClendon, C.L., Torella, R., and Gohlke, H. (2017). Ensemble-and rigidity theory-based perturbation approach to analyze dynamic allostery. J. Chem. Theor. Comput. *13*, 6343–6357.

63. Pfleger, C., Rathi, P.C., Klein, D.L., Radestock, S., and Gohlke, H. (2013). Constraint Network Analysis (CNA): A Python Software Package for Efficiently Linking Biomacromolecular Structure, Flexibility,(thermo-) Stability, and Function (ACS Publications).

64. Thery, F., Eggermont, D., and Impens, F. (2021). Proteomics Mapping of the ISGylation Landscape in Innate Immunity. Front. Immunol. *12*, 720765. https://doi.org/10.3389/fimmu.2021.720765.

65. Giannakopoulos, N.V., Luo, J.K., Papov, V., Zou, W., Lenschow, D.J., Jacobs, B.S., Borden, E.C., Li, J., Virgin, H.W., and Zhang, D.E. (2005). Proteomic identification of proteins conjugated to ISG15 in mouse and human cells. Biochem. Biophys. Res. Commun. *336*, 496–506. https://doi.org/10.1016/j.bbrc.2005.08.132.

66. Zhu, C., Li, J., Tian, C., Qin, M., Wang, Z., Shi, B., Qu, G., Wu, C., and Nan, Y. (2021). Proteomic Analysis of ISGylation in Immortalized Porcine Alveolar Macrophage Cell Lines Induced by Type I Interferon. Vaccines *9*. https://doi.org/10.3390/vaccines9020164.

67. Ganesan, M., Poluektova, L.Y., Tuma, D.J., Kharbanda, K.K., and Osna, N.A. (2016). Acetaldehyde Disrupts Interferon Alpha Signaling in Hepatitis C Virus-Infected Liver Cells by Up-Regulating USP18. Alcohol Clin. Exp. Res. *40*, 2329–2338. https://doi.org/10.1111/acer.13226.

68. Zhang, Z.D., Xiong, T.C., Yao, S.Q., Wei, M.C., Chen, M., Lin, D., and Zhong, B. (2020). RNF115 plays dual roles in innate antiviral responses by catalyzing distinct ubiquitination of MAVS and MITA. Nat. Commun. *11*, 5536. https://doi.org/10.1038/s41467-020-19318-3.

69. Lin, B., Torreggiani, S., Kahle, D., Rumsey, D.G., Wright, B.L., Montes-Cano, M.A., Silveira, L.F., Alehashemi, S., Mitchell, J., Aue, A.G., et al. (2021). Case Report: Novel SAVI-Causing Variants in STING1 Expand the Clinical Disease Spectrum and Suggest a Refined Model of STING Activation. Front. Immunol. *12*, 636225. https://doi.org/10.3389/fimmu.2021.636225.

70. Dzimianski, J.V., Scholte, F.E.M., Bergeron, É., and Pegan, S.D. (2019). ISG15: It's Complicated. J. Mol. Biol. *431*, 4203–4216. https://doi.org/10.1016/j.jmb.2019.03.013.

71. Staib, C., Drexler, I., and Sutter, G. (2004). Construction and isolation of recombinant MVA. Methods Mol. Biol. *269*, 77–100. https://doi.org/10.1385/1-59259-789-0:077.

72. Osei Kuffour, E., Schott, K., Jaguva Vasudevan, A.A., Holler, J., Schulz, W.A., Lang, P.A., Lang, K.S., Kim, B., Häussinger, D., König, R., and Münk, C. (2018). USP18 (UBP43) Abrogates p21-Mediated Inhibition of HIV-1. J. Virol. *92*, 005922-e618. https://doi.org/10.1128/JVI.00592-18.

73. Ketscher, L., Basters, A., Prinz, M., and Knobeloch, K.P. (2012). mHERC6 is the essential ISG15 E3 ligase in the murine system. Biochem. Biophys. Res. Commun. *417*, 135–140. https://doi.org/10.1016/j.bbrc.2011.11.071.

74. Bähr, A., Singer, A., Hain, A., Vasudevan, A.A.J., Schilling, M., Reh, J., Riess, M., Panitz, S., Serrano, V., Schweizer, M., et al. (2016). Interferon but not MxB inhibits foamy retroviruses. Virology *488*, 51–60. https://doi.org/10.1016/j.virol.2015.10.034.

75. Dull, T., Zufferey, R., Kelly, M., Mandel, R.J., Nguyen, M., Trono, D., and Naldini, L. (1998). A third-generation lentivirus vector with a conditional packaging system. J. Virol. *72*, 8463–8471. https://doi.org/10.1128/JVI.72.11.8463-8471.1998.

76. Sunseri, N., O'Brien, M., Bhardwaj, N., and Landau, N.R. (2011). Human immunodeficiency virus type 1 modified to package Simian immunodeficiency virus Vpx efficiently infects macrophages and dendritic cells. J. Virol. *85*, 6263–6274. https://doi.org/10.1128/JVI.00346-11.

77. Mulnaes, D., Porta, N., Clemens, R., Apanasenko, I., Reiners, J., Gremer, L., Neudecker, P., Smits, S.H.J., and Gohlke, H. (2020). TopModel: Template-based protein structure prediction at low sequence identity using top-down consensus and deep neural networks. J. Chem. Theor. Comput. *16*, 1953–1967.

78. Kootstra, N.A., Münk, C., Tonnu, N., Landau, N.R., and Verma, I.M. (2003). Abrogation of postentry restriction of HIV-1-based lentiviral vector transduction in simian cells. Proc. Natl. Acad. Sci. USA *100*, 1298–1303. https://doi.org/10.1073/pnas.0337541100.

79. Hultquist, J.F., Schumann, K., Woo, J.M., Manganaro, L., McGregor, M.J., Doudna, J., Simon, V., Krogan, N.J., and Marson, A. (2016). A Cas9 Ribonucleoprotein Platform for Functional Genetic Studies of HIV-Host Interactions in Primary Human T Cells. Cell Rep. *17*, 1438–1452. https://doi.org/10.1016/j.celrep.2016.09.080.

80. Weisheit, I., Kroeger, J.A., Malik, R., Klimmt, J., Crusius, D., Dannert, A., Dichgans, M., and Paquet, D. (2020). Detection of Deleterious On-Target Effects after HDR-Mediated CRISPR Editing. Cell Rep. *31*, 107689. https://doi.org/10.1016/j.celrep.2020.107689.

81. Yang-Hartwich, Y., Bingham, J., Garofalo, F., Alvero, A.B., and Mor, G. (2015). Detection of p53 protein aggregation in cancer cell lines and tumor samples. Methods Mol. Biol. *1219*, 75–86. https://doi.org/10.1007/978-1-4939-1661-0_7.

82. Georgana, I., Sumner, R.P., Towers, G.J., and Maluquer de Motes, C. (2018). Virulent Poxviruses Inhibit DNA Sensing by Preventing STING Activation. J. Virol. *92*, 021455–e2217. https://doi.org/10.1128/JVI.02145-17.

83. Webb, B., and Sali, A. (2016). Comparative Protein Structure Modeling Using MODELLER. Curr. Protoc. Bioinformatics *54*, 5.6.1–5.6.37. https://doi.org/10.1002/cpbi.3.

84. Pei, J., Kim, B.H., and Grishin, N.V. (2008). PROMALS3D: a tool for multiple protein sequence and structure alignments. Nucleic Acids Res. *36*, 2295–2300. https://doi.org/10.1093/nar/gkn072.

85. Shen, M.Y., and Sali, A. (2006). Statistical potential for assessment and prediction of protein structures. Protein Sci. *15*, 2507–2524. https://doi.org/10.1110/ps.062416606.

86. Chemical Computing Group, U. (2023). Molecular Operating Environment (MOE).

87. van Zundert, G.C.P., Rodrigues, J.P.G.L.M., Trellet, M., Schmitz, C., Kastritis, P.L., Karaca, E., Melquiond, A.S.J., van Dijk, M., de Vries, S.J., and Bonvin, A.M.J.J. (2016). The HADDOCK2.2 Web Server: User-Friendly Integrative Modeling of Biomolecular Complexes. J. Mol. Biol. *428*, 720–725. https://doi.org/10.1016/j.jmb.2015.09.014.

88. Honorato, R.V., Koukos, P.I., Jiménez-García, B., Tsaregorodtsev, A., Verlato, M., Giachetti, A., Rosato, A., and Bonvin, A.M.J.J. (2021). Structural Biology in the Clouds: The WeNMR-EOSC Ecosystem. Front. Mol. Biosci. *8*, 729513.

89. Lu, D., Shang, G., Li, J., Lu, Y., Bai, X.-c., and Zhang, X. (2022). Activation of STING by targeting a pocket in the transmembrane domain. Nature *604*, 557–562.

90. Jorgensen, W.L., Chandrasekhar, J., Madura, J.D., Impey, R.W., and Klein, M.L. (1983). Comparison of simple potential functions for simulating liquid water. J. Chem. Phys. *79*, 926–935. https://doi.org/10.1063/1.445869.

91. Schott-Verdugo, S., and Gohlke, H. (2019). PACKMOL-Memgen: A Simple-To-Use, Generalized Workflow for Membrane-Protein-Lipid-Bilayer System Building. J. Chem. Inf. Model. *59*, 2522–2528. https://doi.org/10.1021/acs.jcim.9b00269.

92. Case, D.A., Cheatham, T.E., 3rd, Darden, T., Gohlke, H., Luo, R., Merz, K.M., Jr., Onufriev, A., Simmerling, C., Wang, B., and Woods, R.J. (2005). The Amber biomolecular simulation programs. J. Comput. Chem. *26*, 1668–1688. https://doi.org/10.1002/jcc.20290.

93. Case, D.A., H.M., A., Belfon, K., Ben-Shalom, I.Y., Berryman, J.T., Brozell, S.R., Cerutti, D.S., Cheatham, T.E., 3rd, Cisneros, G.A., Cruzeiro, V.W.D., et al. (2022). Amber 2022 (University of California).

94. Maier, J.A., Martinez, C., Kasavajhala, K., Wickstrom, L., Hauser, K.E., and Simmerling, C. (2015). ff14SB: Improving the Accuracy of Protein Side Chain and Backbone Parameters from ff99SB. J. Chem. Theor. Comput. *11*, 3696–3713. https://doi.org/10.1021/acs.jctc.5b00255.

95. Dickson, C.J., Walker, R.C., and Gould, I.R. (2022). Lipid21: Complex Lipid Membrane Simulations with AMBER. J. Chem. Theor. Comput. *18*, 1726–1736. https://doi.org/10.1021/acs.jctc.1c01217.

96. Frisch, M.J., G.W.T., Schlegel, H.B., Scuseria, G.E., Robb, M.A., J.R.C., Scalmani, G., Barone, V., Petersson, G.A., H.N., et al. (2016). Gaussian16 (Gaussian Inc.).

97. Bayly, C.I., Cieplak, P., Cornell, W., and Kollman, P.A. (1993). A well-behaved electrostatic potential based method using charge restraints for deriving atomic charges: the RESP model. J. Phys. Chem. *97*, 10269–10280. https://doi.org/10.1021/j100142a004.

98. Wang, J., Wang, W., Kollman, P.A., and Case, D.A. (2006). Automatic atom type and bond type perception in molecular mechanical calculations. J. Mol. Graph. Model. *25*, 247–260. https://doi.org/10.1016/j.jmgm.2005.12.005.

99. Roe, D.R., and Cheatham, T.E., 3rd. (2013). PTRAJ and CPPTRAJ: Software for Processing and Analysis of Molecular Dynamics Trajectory Data. J. Chem. Theor. Comput. *9*, 3084–3095. https://doi.org/10.1021/ct400341p.

100. Pfleger, C., Rathi, P.C., Klein, D.L., Radestock, S., and Gohlke, H. (2013). Constraint Network Analysis (CNA): A Python Software Package for Efficiently Linking Biomacromolecular Structure, Flexibility, (Thermo-) Stability, and Function. J. Chem. Inf. Model. *53*, 1007–1015. https://doi.org/10.1021/ci400044m.

STAR★METHODS

KEY RESOURCES TABLE

REAGENT or RESOURCE	SOURCE	IDENTIFIER
Antibodies		
Rabbit polyclonal anti-V5 Tag	Sigma-Aldrich	Cat# V8137; RRID: AB_261889
Rabbit polyclonal anti-FLAG Tag	Sigma-Aldrich	Cat# F7425; RRID: AB_439687
Rabbit monoclonal anti-HA Tag	Proteintech	Cat# 66006-2-Ig; RRID:AB_2881490
Mouse monoclonal anti-alpha-Tubulin	Sigma-Aldrich	Cat# T6074; RRID: AB_477582)
Goat polyclonal anti-GAPDH	Everest Biotech	Cat# EB06377; RRID: AB_2107455
Rabbit monoclonal anti-USP18	Cell Signaling Technology	Cat# 4813; RRID: AB_10614342
Rabbit polyclonal anti-ISG15	Proteintech	Cat# 15981-1-AP; RRID: AB_2126302
Mouse monoclonal anti-ISG15	Santa Cruz Biotechnology	Cat# sc-166755; RRID: AB_2126308
Rabbit polyclonal anti-STING	Proteintech	Cat# 19851-1-AP; RRID: AB_10665370
Rabbit monoclonal anti-STING	Cell Signaling Technology	Cat# 13647; RRID: AB_2732796
Rabbit monoclonal anti-Phospho-STING (Ser366)	Cell Signaling Technology	Cat# 19781; RRID: AB_2737062
Rabbit monoclonal anti-TBK1	Cell Signaling Technology	Cat# 3504; RRID: AB_2255663
Rabbit monoclonal anti-Phospho-TBK1 (Ser172)	Cell Signaling Technology	Cat# 5483; RRID: AB_10693472
Rabbit monoclonal anti-IRF3	Cell Signaling Technology	Cat# 4302; RRID: AB_1904036
Rabbit monoclonal anti-Phospho-IRF3 (Ser386)	Abcam	Cat# ab76493; RRID: AB_1523836)
Rabbit polyclonal anti-SARS-CoV-2 Nsp3	Cell Signaling Technology	Cat# 88086
Rabbit polyclonal anti-TRIM25	Proteintech	Cat# 12573-1-AP, RRID:AB_2209732
Rabbit polyclonal anti-HERC5	Proteintech	Cat# 22692-1-AP, RRID:AB_2879151
Mouse monoclonal anti-ARIH1	Santa Cruz Biotechnology	Cat# sc-514551
Rabbit polyclonal anti-SOX2	Cell Signaling Technology	Cat# 2748; RRID: AB_823640
Mouse monoclonal anti-OCT4	Santa Cruz Biotechnology	Cat# sc-5279; RRID: AB_628051)
Mouse monoclonal anti-SOX17	R and D Systems	Cat# MAB1924; RRID: AB_2195646
Mouse monoclonal anti-NESTIN	R and D Systems	Cat# MAB1195; RRID: AB_357520
Goat polyclonal anti FOXA2	R and D Systems	Cat# AF2400; RRID: AB_2294104
Rabbit polyclonal anti-PAX6	Invitrogen	Cat# 42–6600; RRID: AB_253354
Mouse monoclonal anti-NCAM(CD56)	Novus	Cat# NB110-59997; RRID: AB_905284
Sheep monoclonal anti-mouse IgG (H + L) secondary antibody, HRP	Cytiva	Cat# NA931; RRID: AB_772210
Donkey monoclonal anti-rabbit IgG (H + L) secondary antibody, HRP	Cytiva	Cat# NA9340; RRID: AB_772191
Mouse monoclonal anti-goat IgG (H + L) secondary antibody, HRP	Santa Cruz Biotechnology	Cat# sc-2354; RRID: AB_628490
Mouse monoclonal anti-rabbit IgG LCS secondary antibody, HRP	Abbkine	Cat# A25022; RRID: AB_2893334
Alexa Fluor 488 goat anti-mouse IgG (H + L)	Invitrogen	Cat# A11029; RRID: AB_138404
Alexa Flour 488 goat anti-rabbit IgG (H + L)	Invitrogen	Cat# A11008; RRID: AB_143165
Alexa Fluor 594 donkey anti-rabbit IgG (H + L)	Invitrogen	Cat# A21207, RRID: AB_141637
Alexa Fluor 594 donkey anti-goat IgG (H + L)	Invitrogen	Cat# A21468, RRID: AB_253587
Bacterial and virus strains		
MVA	Staib et al.[71]	N/A
HIV-1 luciferase reporter virus	Osei Kuffour et al.[72]	N/A

(*Continued on next page*)

Continued

REAGENT or RESOURCE	SOURCE	IDENTIFIER
Chemicals, peptides, and recombinant proteins		
PolyJet™ *In Vitro* DNA Transfection Reagent	SignaGen Laboratories	Cat# SL100688
Anti-HA Affinity Matrix	Sigma-Aldrich	Cat# 11815016001
Protein A/G Magnetic Beads	MedchemExpress	Cat# HY-K0202
Herring Sperm DNA	Promega	Cat# D1811
SR-717	Chin et al.[54]	N/A
Fetal Bovine Serum	PAN-Biotech	Cat# P30-3306
Glutamine	PAN-Biotech	Cat# P04-82100
penicillin-streptomycin	PAN-Biotech	Cat# P06-07100
Blasticidin S hydrochloride	Sigma-Aldrich	Cat# 3513-03-9
Zeocin®	Invitrogen	Cat# 11006-33-0
Protease Inhibitor Cocktail	Merck Millipore	Cat# 539134
Phosphatase Inhibitor Cocktail II	MedchemExpress	Cat# HY-K0022
NuPAGE™ LDS Sample Buffer	Thermo Fisher Scientific	Cat# NP0007
Recombinant Human IFN-Beta	PBL Assay Science	Cat# 11415-1
Cas9-NLS Purified Protein	QB3 Macrolab	https://macrolab.qb3.berkeley.edu/cas9-nls-purified-protein/
Phenylmethanesulfonyl fluoride	Sigma-Aldrich	Cat# 329-98-6
Paraformaldehyde	Sigma-Aldrich	Cat# 30525-89-4
HOECHST	Thermo Fisher Scientific	Cat# 62249
Alt-R HDR Enhancer V2	Integrated DNA Technologies	Cat# 10007910
Y-27632	STEMCELL Technologies	Cat# 72302
STEMdiff™ Trilineage Differentiation Kit	STEMCELL Technologies	Cat# 05230_C
Edit-R CRISPR-Cas9 Synthetic tracrRNA	Dharmacon	https://horizondiscovery.com/en/resources/featured-articles/dharmacon-editr-crispr-cas9-gene-engineering-system
GoTaq polymerase	Promega	Cat# M3005
mTeSR™ Plus	STEMCELL Technologies	Cat# 100-0276
ReLeSR™	STEMCELL Technologies	Cat# 100-0484
P3 primary cell line Kit	Lonza	Cat# V4XP-3032
Matrigel	Corning	Cat# 354277
Critical commercial assays		
Steady-Glo® Luciferase Assay System	Promega	Cat# E2510
RNeasy mini kit	Qiagen	Cat# 74004
Revert Aid H-Minus First Strand cDNA Synthesis kit	Thermo Fisher Scientific	Cat# K1631
SYBR Green PCR Master Mix	Thermo Fisher Scientific	Cat# 4309155
QuantiTect SYBR Green RT-PCR Kit	Qiagen	Cat# 204243
Direct-zol RNA Kit	ZYMO-Research	Cat# R2050
QUANTI-Blue™ Solution	InvivoGene	Cat# rep-qbs
PrimeTime™ One-Step RT-qPCR Master Mix, 1 mL	Integrated DNA Technologies	Cat# 10007065
Deposited data		
MD simulation data	researchdata.hhu.de	https://doi.org/10.25838/d5p-50
Experimental models: Cell lines		
HEK293T	ATCC	Cat# CRL-3216; RRID: CVCL_0063
HEK293A	Invitrogen	Cat# R70507; RRID: CVCL_6910

(*Continued on next page*)

Continued

REAGENT or RESOURCE	SOURCE	IDENTIFIER
THP-1	ATCC	Cat# TIB-202; RRID: CVCL_0006
HEK-Blue™ IFN-α/β cells	InvivoGene	Cat# hkb-ifnab
THP-1.pLV2 (pLentiCRISPRv2 empty vector (pLV2)) cells	Osei Kuffour et al.[50]	N/A
ISG15 knockout THP-1 cells	Osei Kuffour et al.[50]	N/A
STING knockout THP-1 cells	Mankan et al.[16]	N/A
Reconstituted STING THP-1 cells	This paper	N/A
STING-K289R PEIi003-A-1	This paper	N/A
PBMCs	German Red Cross Blood Donor Service Baden-Württemberg Hessen, Germany	N/A
PEIi003-A	Fuchs et al.[57]	RRID: CVCL_YC51
MHHi008-B	Haase et al.[59]	RRID: CVCL_VS.39
Oligonucleotides		
qRT-PCR primers	Table S1	N/A
Edit-R Modified Synthetic crRNA targeting STING: 5′-ACTCTTCTGCCGGACACTTG	This paper	N/A
Forward primer for amplification of *STING* locus: 5′-AGACCCCATTAGGGTGGCC-3′	This paper	N/A
Reserve primer for amplification of *STING* locus: 5′-AGACCCCATTAGGGTGGCC-3′	This paper	N/A
Forward primer for amplification of STING alleles: 5′-AGACCCCATTAGGGTGGCC-3′	This paper	N/A
Reserve primer for amplification of STING alleles: 5′-CTGCCCTCCAGCCTATCAAC-3′	This paper	N/A
Probe for STING alleles: 5′-TCTCAGAACAACTGCCGCCTCATT-3	This paper	N/A
ssDNA homologous recombination template:/Alt-R-HDR1/T*C*A AGC TGG CTT TAG CCG GGA GGA TAG GCT TGA GCA GGC CCG ACT CTT CTG CCG GAC ATT GGA GGA CAT CCT GGC AGA TGC CCC TGA GTC TCA GAA C*A*A/Alt-R-HDR2	This paper	N/A
Recombinant DNA		
pLOC empty vector	Thermo Fisher Scientific	N/A
pLOC-USP18	Osei Kuffour et al.[72]	N/A
pLOC-USP18-C64A	Osei Kuffour et al.[72]	N/A
pLOC-USP18-C64S	Osei Kuffour et al.[72]	N/A
pLOC-USP18-V5	Osei Kuffour et al.[72]	N/A
pLOC-ISG15	Horizon	Vector clone ID: PLOHS_100011506
pLOC-UBE1L (E1)	Ketscher et al.[73]	N/A
pLOC-UBCH8 (E2)	Ketscher et al.[73]	N/A
pSIN.PPT.CMV.Luc.IRES.GFP	Bähr et al.[74]	N/A
pMDLg/pRRE	Dull et al.[75]	RRID: Addgene_12251
pRSV-Rev	Dull et al.[75]	RRID: Addgene_12253
pMD.G	Dull et al.[75]	N/A
pcDNA6/myc-His-VPX	Sunseri et al.[76]	N/A
pMDLx/pRRE	Sunseri et al.[76]	N/A

(*Continued on next page*)

Continued

REAGENT or RESOURCE	SOURCE	IDENTIFIER
psPAX2	NIH, AIDS Reagent Program repository	RRID: Addgene_12260
pcDNA3.1-FLAG-ubiquitin	Klaus Harbers	N/A
pLOC-STING-HA	This paper	N/A
pLOC-STING-K0-HA (A20, A137, A150, A224, A236, A289, A338, A347, A370)	This paper	N/A
pLOC-STING-K0-A20K-HA (replace A20 to K20 at pLOC-STING-K0-HA)	This paper	N/A
pLOC-STING-K0-A137K-HA	This paper	N/A
pLOC-STING-K0-A150K-HA	This paper	N/A
pLOC-STING-K0-A224K-HA	This paper	N/A
pLOC-STING-K0-A236K-HA	This paper	N/A
pLOC-STING-K0-A289K-HA	This paper	N/A
pLOC-STING-K0-A338K-HA	This paper	N/A
pLOC-STING-K0-A347K-HA	This paper	N/A
pLOC-STING-K0-A370K-HA	This paper	N/A
pLOC-STING-K224R-HA (replace K224 to R224 at pLOC-STING-HA)	This paper	N/A
pLOC-STING-K236R-HA	This paper	N/A
pLOC-STING-K289R-HA	This paper	N/A
pLOC-STING-K338R-HA	This paper	N/A
pLOC-STING-K347R-HA	This paper	N/A
pLOC-STING-K370R-HA	This paper	N/A
pLOC-STING-K6R-HA (R224, R236, R289, R338, R347, R370)	This paper	N/A
pLOC-STING-K5R-R224K-HA (replace R224 to K224 at pLOC-STING-K6R-HA)	This paper	N/A
pLOC-STING-K5R-R236K-HA	This paper	N/A
pLOC-STING-K5R-R289K-HA	This paper	N/A
pLOC-STING-K5R-R338K-HA	This paper	N/A
pLOC-STING-K5R-R347K-HA	This paper	N/A
pLOC-STING-K5R-R370K-HA	This paper	N/A
pLOC-STING-S366A-HA	This paper	N/A
pLOC-STING-V155M-HA	This paper	N/A
pLOC-STING-K6R-V155M-HA	This paper	N/A
pLOC-STING-K289R-V155M-HA	This paper	N/A
Software and algorithms		
GraphPad Prism 8	GraphPad	https://www.graphpad.com
ImageJ V 1.53	ImageJ	https://imagej.nih.gov/ij
SP8 confocal microscope software	Leica	https://www.leica-microsystems.com/products/confocal-microscopes/p/leica-tcs-sp8/
Modeller, v. 9.19	Modeller	https://salilab.org/modeller/
PROMALS3D	PROMALS3D	http://prodata.swmed.edu/promals3d
TopModel	TopModel[77]	https://cpclab.uni-duesseldorf.de/topsuite/topmodel.php
MOE2022.09	Chemical Computing Group	https://www.chemcomp.com/
HADDOCK 2.4	Bijvoet Center for Biomolecular Research	https://wenmr.science.uu.nl/haddock2.4/
Constraint Network Analysis software	Constraint Network Analysis software	https://cpclab.uni-duesseldorf.de/cna/

RESOURCE AVAILABILITY

Lead contact

Further information and requests for resources and reagents should be directed to and will be fulfilled by the lead contact, Carsten Münk (carsten.muenk@med.uni-duesseldorf.de).

Materials availability

All unique/stable reagents generated in this study are available from the lead contact with a completed materials transfer agreement.

Data and code availability

- All data reported in this paper will be shared by the lead contact upon request.
- This paper does not report original code.
- Any additional information required to reanalyze the data reported in this paper is available from the lead contact upon request.

EXPERIMENTAL MODEL AND STUDY PARTICIPANT DETAILS

Cell lines and culture conditions

HEK293T cells (American Type Culture Collection (ATCC)) and HEK293A cells (Invitrogen) were cultured in Dulbecco's Modified Eagle Medium (DMEM) (PAN-Biotech) supplemented with 10% fetal bovine serum (FBS) (PAN-Biotech), 2 mM L-glutamine (PAN-Biotech), and 100 U/ml penicillin-streptomycin (PAN-Biotech). THP-1 cells were obtained from ATCC and maintained in Roswell Park Memorial Institute (RPMI) 1640 (Gibco) containing 10% FBS, 2 mM L-glutamine, and 100 U/ml penicillin-streptomycin. ISG15 knockout THP-1 cells (THP-1.ISG15KO-E1 and THP-1.ISG15KO-E2; made with pLentiCRISPRv2 containing the specific ISG15 single-guide RNA (sgRNA) sequences targeting exon 1 (E1) and exon 1 (E2) of the *ISG15* gene) and THP-1.pLV2 (pLenti-CRISPRv2 empty vector (pLV2)) cells were described before.[50] STING knockout THP-1 cells were obtained as a gift from Veit Hornung.[16] HEK-Blue IFN-α/β cells (Invivogene) were maintained in DMEM supplemented with 10% FBS, 2 mM L-glutamine, 100 U/ml penicillin-streptomycin, 30 μg/mL of blasticidin S hydrochloride (Sigma-Aldrich), and 100 μg/mL of Zeocin (Invivogene). Induced pluripotent stem cells were maintained on Matrigel (Corning) coated dishes in mTeSR Plus (STEMCELL Technologies) at 37°C and 5% CO_2, 21% O_2 in a humidified atmosphere. Once per week cells have been splitted in ration of 1:4 -1:6 using ReLeSR (STEMCELL Technologies). The differentiation of iPS cells to hematopoietic progenitor cells was performed according to the protocol published by Sontag et al.[58] The human peripheral blood mononuclear cells (PBMCs) were isolated from human buffy coats of anonymous blood donors purchased from the German Red Cross Blood Donor Service Baden-Württemberg Hessen, Germany.

METHOD DETAILS

Constructs and transfection

pLOC-USP18, pLOC-USP18-C64A (active site mutant), pLOC-USP18-C64S (active site mutant), and pLOC-USP18-V5 plasmids were described before.[72] HA-tagged STING and its single/multiple-amino-acid mutants were cloned into pLOC vector (Thermo Fisher Scientific) using SpeI and AscI restriction sites. pLOC-ISG15 plasmid were obtained from Horizon (Vector clone ID: PLOHS_100011506). E1 (UBE1L) and E2 (UBCH8) plasmids were kind gifts from Klaus-Peter Knobeloch.[73] FLAG-tagged ubiquitin expression plasmid was kind gift from Klaus Harbers. pSIN.PPT.CMV.Luc.IRES.GFP,[74,78] pMDLg/pRRE,[75] pRSV-Rev,[75] pMD.G,[75] pcDNA6/myc-His-VPX,[76] and pMDLx/pRRE[76] plasmids have been described before.[72] The HIV-1 construct psPAX2 was obtained from the NIH, AIDS Reagent Program repository. For transfection, PolyJet *in vitro* DNA transfection reagent (SignaGen Laboratories) was used according to the manufacturer's protocol.

Virus production and transduction

Modified vaccinia virus Ankara (MVA) (cloned isolate F6) at 582nd passage on chicken embryo fibroblasts (CEF) were routinely propagated, purified by two consecutive ultracentrifugation steps through a 36% (w/v) sucrose cushion and titrated following standard methodology.[71] HIV-1 luciferase reporter viruses were generated as described before.[72] HIV-1 luciferase reporter viruses were produced by co-transfecting HEK293T cells with 600 ng of pMDLg/pRRE or pMDLx g/pRRE, 150 ng of pMD.G, 250 ng of pRSV-Rev, and 600 ng of pSIN.PPT.CMV.Luc.IRES.GFP with or without pcDNA6/myc-His-VPX. Viral supernatants were harvested 48 h post-transfection, purified, concentrated over a 20% (w/v) sucrose cushion, resuspended in fresh RPMI medium, and stored in −80°C. THP-1 cells were transduced with HIV-1 luciferase reporter viruses for the indicated time and the efficiency of HIV-1 infection was analyzed by a Steady-Glo Luciferase Assay System (Promega) according to the manufacturer's instructions.

Generation of reconstituted STING THP-1 cells

Reconstituted STING THP-1 cells were generated by transduction of STING knockout THP-1 cells with lentiviral vectors that were made by co-transfection of 600 ng of lentiviral pLOC empty vector (pEV) or pLOC-STING-HA (wild-type and mutant) together with

600 ng of psPAX2, 250 ng pRSV-Rev, and 150 ng of pMD.G in HEK293T cells. Viral particles were concentrated by ultracentrifugation at 14,000 × rpm for 2 h at 4°C and resuspended in RPMI. The cells were spinoculated at 1200 × g for 2 h at 30°C and selected using blasticidin S hydrochloride.

Generation of STING_K289R knock-in cells

Ribonucleoprotein complexes for the CRISPR/Cas9-mediated knock-in were generated as described previously.[79] Briefly, 200 pmol Edit-R Modified Synthetic crRNA targeting *STING* (target sequence: 5′-ACTCTTCTGCCGGACACTTG-3' (Integrated DNA Technologies, IDT), 200 pmol Edit-R CRISPR-Cas9 Synthetic tracrRNA (Dharmacon), and 40 pmol Cas9-NLS (QB3 Macrolab) were assembled *in vitro*. The LONZA 4D-Nucleofector X Unit was used to deliver ribonucleoprotein complexes together with 100 pmol of ssDNA homologous recombination template (with 5' homology arm length 36 and 3' homology arm length 40,/Alt-R-HDR1/T*C*A AGC TGG CTT TAG CCG GGA GGA TAG GCT TGA GCA GGC CCG ACT CTT CTG CCG GAC ATT GGA GGA CAT CCT GGC AGA TGC CCC TGA GTC TCA GAA C*A*A/Alt-R-HDR2) into 4 x 10^5 pluripotent stem cell line PEIi003-A,[57] passage 20. Nucleofection was performed with P3 primary cell line Kit (Lonza), applying program CM-113 following the manufacturer's instruction. To increase KI efficiency after nucleofection the cells were kept for 24 h at 32°C in medium containing 1:200 Alt-R HDR Enhancer V2 (IDT) and Y-27632 at final concentration of 10 μM. Single cell clones were analyzed by PCR amplification of *STING* locus utilizing GoTaq polymerase (Promega) and primer pair FW_AGACCCCATTAGGGTGGCC, RV_ CTGCCCTCCAGCCTATCAAC. Sanger sequencing confirmed the KI. Presence of both alleles was confirmed by quantitative genomic PCR as described previously[80] applying the primers genomic FW_AGACCCCATTAGGGTGGCC and genomic RV_CTGCCCTCCAGCCTATCAAC in combination with probe TCTCAGAACAACTGCCGCCTCATT in PrimeTime One-Step RT-qPCR Master Mix. Cell mRNA was isolated with Direct-zol RNA Kit (ZYMO-Research). Quantitative reverse transcription PCR (RT-qPCR) was performed with QuantiTect SYBR Green RT-PCR Kit. *RPL13A* served as housekeeping gene. The PCR conditions were as follows: one cycle of reverse transcription for 30 min at 50°C. Followed by initial denaturation/heat activation for 15 min at 95°C, 45 cycles of denaturation for 15 s at 95°C, annealing for 15 s at 56°C, elongation for 1 min at 72°C. Dissociation analysis was performed subsequently for 15 s at 95°C, followed by 15 s at 60°C and 15 s at 95°C. The qPCR was performed on BIORAD CFX 384 Real-Time System, C1000 Touch Thermal Cycler.

Immunocytochemistry

The immunofluorescence staining of pluripotency markers (OCT4 and SOX2) and expression of pluripotency markers OCT4, SOX2, and NANOG were determined as described previously.[57] STING-K289R PEIi003-A-1 iPSCs were differentiated using the STEMdiff Trilineage Differentiation Kit (STEMCELL Technologies) and stained for expression of gene markers characterizing three germ layers (ectoderm, mesoderm, and endoderm) as described previously.[57] Briefly, cells were treated for 20 min at room temperature with 2% paraformaldehyde and then for 15 min at room temperature with 0.5% Triton X-100 1 × PBS. Cells were blocked for 60 min at room temperature in 2% bovine serum albumin. followed by subsequent incubation with primary antibodies for 1 h at room temperature. After washing s incubation with secondary antibodies for 1 h was performed. Nuclei were stained with HOECHST (1:5000) for 2 min before mounting. All images were acquired with SP8 confocal microscope (Leica).

Immunoblot analysis

Cells were lysed in mild lysis buffer (50 mM Tris-HCl [pH 8], 150 mM NaCl, 0.8% NP-40, 10% glycerol, 1mM phenylmethanesulfonyl fluoride solution [Sigma-Aldrich], a tablet of protease inhibitor cocktail (Merck Millipore) and 1% phosphatase inhibitor cocktail (MedChemExpress)) or radioimmunoprecipitation assay buffer (RIPA buffer) (25 mM Tris-HCl [pH 7.6], 150 mM NaCl, 1% NP-40, 1% sodium deoxycholate, 0.1% SDS, a tablet of protease inhibitor cocktail and 1% phosphatase inhibitor cocktail). Cell lysates were subjected to SDS-PAGE followed by immunoblot analysis with the appropriate antibodies.

ISGylation and ubiquitination analysis

For analyzing ISGylation of STING, HEK293A cells were transfected with the indicated plasmids, or either reconstituted STING THP-1 cells or wildtype THP-1 cells that were stimulated with IFN-β (PBL Assay Science), 3.6 μM STING agonist SR-717 (STING agonist SR-717 was synthesized according to the described method),[54] transfected with 4 μg/mL herring sperm DNA (HS-DNA), or infected with HIV-1 for indicated times. For analyzing the ubiquitination of STING, HEK293A cells were transfected with STING plasmids and FLAG-ubiquitin expression plasmid for 30 h. Cells were harvested and lysed for 20 min on ice with 400 μL lysis buffer. Proteins were subsequently cleared by centrifugation. Cell lysates (360 μL) were incubated with either 10 μL of anti-HA affinity matrix (Sigma-Aldrich), or with 25 μL protein A/G magnetic beads (MedchemExpress) plus anti-STING antibody (1 μg) (Proteintech) or anti-ISG15 (1 μg) (Santa Cruz Biotechnology). The immunoprecipitates were washed three times by 1 mL lysis buffer. Bound proteins were eluted by boiling the beads for 5 min at 95°C in reducing reagent. The rest of the lysates were subject to immunoblot analysis to detect the expression of target proteins and the immunoprecipitates were subsequently immunoblotted for respective antibodies. To avoid the noise of heavy chains, the IPKine HRP, Mouse Anti-Rabbit IgG LCS (Insight Biotechnology, Abbkine Scientific) secondary antibody was used for the immunoprecipitation.

Analyses of STING oligomerization and dimerization

Analysis of STING oligomerization, HEK293A cells that were transfected with wild-type or mutant STING for 24 h or reconstituted STING THP-1 cells were stimulated with 3.6 μM STING agonist SR-717 for 2 h. Cells were harvested and lysed for 20 min on ice

with mild lysis buffer. The lysates were cleared by centrifugation. The supernatant in a sample buffer containing non-denaturing reagents was subject into native PAGE for oligomerization detection.[12,81] Analysis of STING dimerization was performed as described previously.[82] The cell lysates were mixed with NuPAGE LDS sample buffer (Thermo Fisher Scientific) and directly analyzed by SDS-PAGE. Immunoblotting was performed with antibody against STING.

Type I interferon production assay

HEK-Blue IFN-α/β cells were used to examine the release of interferon from mock-treated, HIV-1-infected, MVA-infected, HS-DNA-transfected, STING agonist SR-717-stimulated THP-1 cells, or transfected HEK293A cells according to the manufacturer's instructions. For the assay, 20 μL of the supernatant of mock-treated, infected, stimulated THP-1 cells, or transfected HEK293A cells were added to a 96-well plate followed by 180 μL of HEK-Blue IFN-α/β cells suspension (5.0×10^4 cells per well) and incubated at 37°C in 5% CO_2 for 24 h. 20 μL of supernatants from HEK-Blue IFN-α/β cells were added to 180 μL QUANTI-Blue Solution (InvivoGene) and incubated at 37°C for 1 h. The colorimetric reaction was determined using a spectrophotometer at 630 nm.

Quantitative reverse transcription PCR (RT-qPCR)

Total RNA was extracted from cells using Qiagen RNeasy mini kit (Qiagen), and the first-strand cDNA was reversed-transcribed with Revert Aid H-Minus First Strand cDNA Synthesis kit (Thermo Fisher Scientific Inc.). Gene expression of *IFNB1*, *ISG54*, *ISG15*, *CXCL10*, *TNF-α*, and *GAPDH* was examined with the Applied Biosystems ViiA 7 Real-Time PCR System (Thermo Fisher Scientific Inc.) by using 1 x SYBR Green PCR Master Mix (Thermo Fisher Scientific). The data were analyzed using the comparative threshold cycle (C_T) mean and normalized to GAPDH.

For assessment of the pluripotent state by *OCT4*, *SOX2* and *NANOG* expression, *RPL13A* served as house-keeping gene. The PCR conditions were as follows: one cycle of reverse transcription for 30 min at 50°C. Followed by initial denaturation/heat activation for 15 min at 95°C, 45 cycles of denaturation for 15 s at 95°C, annealing for 15 s at 56°C, elongation for 1 min at 72°C. Dissociation analysis was performed subsequently for 15 s at 95°C, followed by 15 s at 60°C and 15 s at 95°C. The same protocol was applied for amplification of *CD31*, *CD34*, and *ISG54* mRNA levels from hematopoietic progenitor cells, with *RPL13A* as housekeeping gene. The sequences of primers for RT-qPCR analysis were included in Table S1.

Homology modeling

A model of the human STING dimer was generated based on the cryo-EM structure of the full-length chicken STING in the cGAMP-bound dimeric state (PDB-ID: 6NT7)[9] using Modeller, v. 9.19.[83] The alignment was generated using Modeller, v. 9.19,[83] and further verified using PROMALS3D.[84] Water molecules, ligands, and crystallization buffer components in the template were removed. A total of 50 models were generated, and the best structure was chosen based on the DOPE potential[85] and visual inspection. ISG15 was modeled using TopModel.[77] Here, the sequence up to the ligation site was considered. The best resulting model was used for further experiments.

Docking

All proteins were protonated using MOE2022.09.[86] Docking of ISG15 to STING was performed using the HADDOCK 2.4 webserver (https://wenmr.science.uu.nl/haddock2.4/).[87,88] One ISG15 was docked to STING using default parameters, with the exception that K289 of STING and G157 of ISG15 were characterized as active residues and buried active residues were not removed from the selection. The largest and second-best ranked cluster was selected. In comparison to the best-ranked cluster, the carboxy group of G157 of ISG15 was placed closer to K289 of STING (Figure S4), favoring the construction of a covalent bond between both residues. ISG15 was then placed symmetrically at both subunits of the STING dimer. Dimers of dimers of ISG15-bound STING are based on the human cryo-EM structure (PDB ID: 7SII),[89] to which ISGylated STING dimers were aligned.

Molecular dynamics simulations of STING bound to ISG15

For MD simulations, the ligand cGAMP was placed within the orthosteric binding site of STING by aligning the cryo-EM structure of the full-length chicken STING in the cGAMP-bound dimeric state (PDB-ID: 6NT7)[9] to our model. The dimer of dimers of ISGylated STING was treated similarly. The ISGylated STING was then placed in a rectangular box of TIP3P water[90] and embedded in a membrane of 1-palmitoyl-2-oleoyl-*sn*-glycero-3-phosphocholine (POPC) using Packmol-Memgen[91] with the edge of the box at least 12 Å away from solute atoms. KCl was added to a concentration of 150 mM, and the system was neutralized using K^+ ions. The AMBER22 package of molecular simulations software[92,93] in combination with the ff14SB force field[94] for the protein and the Lipid21 force field[95] for lipids were used. Electrostatic potentials of the ligand and the covalently connected lysine and glycine were generated using Gaussian16[96] at the HF-6-31G* level of theory. For lysine and glycine, amines and carboxy groups were capped using ACE and NME, respectively, during this procedure. Charges of the cGAMP ligand were calculated according to the RESP procedure[97] using default parameters, as implemented in antechamber.[98] For lysine and glycine, parameters were created using residuegen, as implemented in Amber22[93] by applying predefined backbone charges for Amber noncharged residues to both residues.

For MD simulations, initially, a combination of steepest descent and conjugate gradient minimization was performed while lowering the positional harmonic restraints on protein and ligand atoms from 25 kcal mol^{-1} $Å^{-2}$ to zero. The system was then heated stepwise to 100 K during 5 ps of NVT-MD simulations, followed by 115 ps of NPT-MD simulations to heat the system to 300 K. During these

steps, harmonic restraints with a force constant of 25 kcal mol^{-1} $Å^{-2}$ were applied to protein and ligand atoms. Subsequently, the restraints were gradually reduced to zero during NPT-MD simulations.

10 replicas of production runs of 750 ns length were performed. Conformations were extracted every 1 ns using CPPTRAJ.[99] CPPTRAJ was also used to compute contact maps and minimum distances using the "nativecontacts" command. To quantify average interaction percentages, a minimum distance <4 Å was considered. CPPTRAJ was also used to compute a 2D root-mean-square deviation (2DRMSD) between STING conformations of the trajectories. Hydrogen bonds between two neighboring ISG15s were computed via the "hbond" command using default parameters.

Constraint network analysis (CNA)

The Constraint Network Analysis (CNA) software package uses a graph theory-based approach to identify floppy and rigid substructures during constraint dilution simulations. This results in stability maps, which can be used to calculate the flow of rigidity percolation through the protein, which in short can be used to quantify the strength of dynamic allostery effects.[62] We performed perturbation runs as implemented in CAN[100] to investigate a potential coupling through the constraint network between ISG15 and the ligand binding site. The perturbation approach[62] performs constraint dilution simulations in the absence and presence of ISG15 and, thereby, calculates $\Delta G_{i,CNA}$, the per-residue decomposition of the free energy associated with the change in biomolecular stability due to the removal of ISG15 indicating the effect of ISG15 on a residue in terms of changes in structural rigidity. The cooperative free energy $\Delta\Delta G_{CNA}$ was calculated via Equation 1.

$$\Delta\Delta G_{CNA} = \Delta G_{ISG15+cGAMP} - (\Delta G_{ISG15} + \Delta G_{cGAMP}) \quad \text{(Equation 1)}$$

where ISG15, cGAMP, or ISG15 + cGAMP were removed from the system after omitting the first 20% of conformations for each replica resulting in three different perturbation runs.[62] This resulted in mean ΔG energies of 22.29 kcal mol^{-1}, 32.59 kcal mol^{-1}, and 146.59 kcal mol^{-1} for ISG15, cGAMP, and ISG15 + cGAMP, respectively, yielding a positive $\Delta\Delta G_{CNA}$.

QUANTIFICATION AND STATISTICAL ANALYSIS

Data were analyzed using GraphPad Prism version 8 (GraphPad Software, Inc., La Jolla, USA). The study groups were compared using one-way analysis of variance (ANOVA) or two-tailed Student's t-test, and a p value of < 0.05 was considered statistically significant. The data represent means ± the standard deviation (SD), as indicated in the figures. Statistical significance was represented as: not significant (ns), *$p < 0.05$, **$p < 0.01$, ***$p < 0.001$, and ****$p < 0.0001$.